Lithos 112 (2009) 118–136

Contents lists available at ScienceDirect

Lithos

journal homepage: www.elsevier.com/locate/lithos

On the composition of ocean island basalts (OIB): The effects of lithospheric thickness variation and mantle metasomatism

Emma R. Humphreys [1], Yaoling Niu *

Department of Earth Sciences, Durham University, Durham DH1 3LE, UK

ARTICLE INFO

Article history:
Received 29 June 2008
Accepted 29 April 2009
Available online 6 June 2009

Keywords:
Ocean islands
Intra-plate magmatism
OIB compositions
Lithospheric thickness control
Mantle metasomatism

ABSTRACT

We have examined island-averaged geochemical data for 115 volcanic islands with known eruption ages and ages of the underlain lithosphere from the Pacific, Atlantic and Indian Oceans. These age data allow calculation of the lithosphere thickness at the time of volcanism. After correcting the basalts (including alkalic types) (<53% SiO_2) for fractionation effect to $Mg^{\#} = 0.72$, we found that the island-averaged Si_{72} and Al_{72} decrease whereas Fe_{72}, Mg_{72}, Ti_{72} and P_{72} increase with increasing lithosphere thickness. The island-averaged $[La/Sm]_{CN}$ and $[Sm/Yb]_{CN}$ ratios also increase with increasing lithosphere thickness. These statistically significant trends are most consistent with the interpretation that the mean extent of melting decreases whereas the mean pressure of melting increases with increasing lithosphere thickness. This is physically consistent with the active role the lithosphere plays in limiting the final depth of intra-oceanic mantle melting. That is, beneath a thin lithosphere, a parcel of mantle rises to a shallow level, and thus melts more by decompression with the aggregated melt having the property of high extent and low pressure of melting. By contrast, a parcel of mantle beneath a thick lithosphere has restricted amount of upwelling, and thus melts less by decompression with the aggregated melt having the property of low extent and high pressure of melting. This demonstrates that oceanic lithosphere thickness variation exerts the first-order control on the geochemistry of ocean island basalts (OIB). Variation in initial depth of melting as a result of fertile mantle compositional variation and mantle potential temperature variation can influence OIB compositions, but these two variables must have secondary effects because they do not overshadow the effect of lithosphere thickness variation that is prominent on a global scale. The mantle potential temperature variation beneath ocean islands cannot be constrained with the existing data. Fertile mantle source heterogeneity is required to explain the large OIB compositional variation on a given island, between islands and between island groups. The OIB mantle source heterogeneity must have multiple origins, but an incipient melt in the seismic low-velocity zone and its metasomatic lithologies in the lithosphere are best candidates that contribute to the incompatible element enriched OIB geochemistry on two different time scales: (1) melt–lithosphere interaction during OIB magmatism, and (2) recycled metasomatized lithosphere in the OIB source regions.

1. Introduction

The origin of mid-ocean ridge basalts (MORB) and island arc basalts (IAB) is reasonably well understood as a result of plate tectonic processes operating at plate boundaries. The plate tectonics theory, however, cannot readily explain the widespread basaltic volcanism occurring in the interiors of tectonic plates. Intra-plate volcanic activities include those that produce ocean islands, seamounts and oceanic plateaus in ocean basins and flood basalt provinces as well as basaltic rocks in other continental settings.

Parallel to the development of the plate tectonics theory (Wilson, 1963a,b; McKenzie and Parker, 1967; Morgan, 1968), Wilson (1963a,b) interpreted intra-plate volcanic centres such as Hawaii as "hotspots" derived from a relatively fixed source in the mantle that is deeper than, and thus unaffected by, the moving Pacific plate. Morgan (1971, 1972) advocated further that hotspots were surface manifestations of cylindrical plumes derived from the convective lower mantle, presumably initiated at the core–mantle boundary. Although the mantle plume hypothesis remains to be verified, the success of laboratory (e.g., Campbell and Griffiths, 1990) and numerical (e.g., Davies, 1999) simulations in generating "mantle plumes" makes the hypothesis physically plausible. In fact, mantle plumes have been widely invoked to explain many intra-plate volcanic phenomena, particularly those large igneous provinces (LIPs) characterized by

* Corresponding author.
E-mail address: Yaoling.Niu@durham.ac.uk (Y. Niu).
[1] Present address: Department of Earth Sciences (PhD candidate), University of Bristol, Bristol BS8 1RJ, UK; also The Natural History Museum, Cromwell Road, London, SW7 5BD, UK.

0024-4937/$ – see front matter © 2009 Elsevier B.V. All rights reserved.
doi:10.1016/j.lithos.2009.04.038

voluminous mantle melts emplaced over a short time period (e.g., White and McKenzie, 1989; Campbell and Griffiths, 1990; Griffiths and Campbell, 1990; Duncan and Richards, 1991; Coffin and Eldholm, 1994; Courtillot et al., 2003). As a result, the mantle plume hypothesis has imperceptibly become the "answer" to all the intra-plate volcanism (See Niu, 2005a). The mantle plume hypothesis has gained considerable support in the past decades primarily through geochemical studies of ocean island basalts (OIB). The mostly passive upwelling beneath ocean ridges suggests that MORB sample the shallowest upper mantle (e.g., McKenzie and Bickle, 1988). The overall depleted composition of MORB further suggests that the shallowest mantle is geochemically depleted (e.g., Zindler and Hart, 1986; Hofmann, 1988). It follows that the geochemically enriched OIB must have derived from less depleted or even enriched mantle sources in the deep mantle, perhaps in the lower mantle (e.g., Zindler and Hart, 1986), leading to the conjecture of a mantle plume origin for OIB.

The mantle plume hypothesis has also received challenges in more recent years (e.g., Smith and Lewis, 1999; Anderson, 2002; Hamilton, 2002; Foulger, 2005), and the "great plume debate" (GPD) is currently rather heated (e.g., Foulger et al., 2005; Campbell, 2005; Kerr, 2005; Niu, 2005a; Davies, 2005; Foulger, 2005). One of the focal points of the debate is whether OIB are indeed products of deep-rooted mantle plumes or shallow mantle melting anomalies as a result of fertile mantle compositional heterogeneities (Anderson and Natland, 2005) triggered by some poorly understood aspects of plate tectonics (Anderson, 2005; Anderson and Natland, 2005; Niu, 2005b). Geophysical techniques such as seismic tomography have the potential to detect whether cylindrical plumes may indeed exist and extend deep into the lower mantle (Montelli et al., 2004), but they do not yet have the resolving power to prove or disprove the plume hypothesis (Julian, 2005). Therefore, the petrology and geochemistry of OIB remain the primary means used to address relevant issues.

The petrology of OIB can be used to infer mantle potential temperatures (e.g., Herzberg and O'Hara, 2002), which must be high if the OIB sources are derived from deep-rooted thermal mantle plumes, but should be low if the OIB sources are enriched materials with reduced solidus in the shallow mantle (Niu, 2005a). While this concept is straightforward, the calculated mantle potential temperatures are model dependent (e.g., Green et al., 2001; Green and Falloon, 2005; Putirka, 2005; Herzberg et al., 2007). The geochemistry of mantle derived melts is useful in tracing the compositions and histories of mantle source materials (e.g., Gast, 1968; Armstrong, 1968; O'Nions et al., 1979; Allègre et al., 1983), but it cannot resolve whether the source material originates from deep mantle "plumes" or represents passive compositional heterogeneities in the shallow mantle. Noble gas isotopes have been widely considered to be diagnostic in this regard (e.g., Farley et al., 1992; Hart et al., 1992; McKenzie and O'Nions, 1995; Hanan and Graham, 1996; Albarède, 1998; Castillo et al., 2007), but their interpretations may not be unique (e.g., Meibom and Anderson, 2003; Parman et al., 2005; Porcelli and Elliott, 2008). In short, OIB vary considerably in composition (major and trace elements and isotopes) from one volcanic island to another and from one group of islands to another group. Such compositional variation is conceivably the compound effect of mantle source compositional variation, extent and depth of melting, melt–solid interaction during ascent in the mantle and complex magma differentiation processes at crustal levels. Therefore, to genuinely understand OIB petrogenesis in particular and to resolve the mantle plume debate in general require identifying the effect of each of these processes.

In this paper, we report the results of this effort. We demonstrate that the oceanic lithosphere thickness variation exerts the first-order control on the geochemistry of OIB on a global scale despite other effects such as fertile mantle compositional heterogeneity. That is, the lithosphere thickness limits the mean extent and pressure (depth) of melting.

2. The philosophy

Despite "microscopic" complexities in the generation and evolution of mantle derived melts, macroscopically, mantle melting is a physical process. Therefore, mantle melting must leave geochemical imprint on the melting product that reflects the physical controls. This concept has been well illustrated by MORB studies. For example, MORB define distinctive chemical trends between slow and fast spreading ridges (Niu and Batiza, 1993), and MORB compositional variation correlates with plate separation rate variation (Niu and Hékinian, 1997; Rubin and Sinton, 2007) and with ocean ridge axial depth variation on local (Batiza et al., 1988; Brodholt and Batiza, 1989; Batiza and Niu, 1992; Niu and Batiza, 1994; Niu et al., 2001) and global scales (Dick et al., 1984; Klein and Langmuir, 1987; Niu and O'Hara, 2008). For intra-plate ocean island magmatism, the only known or best constrained physical variable is the thickness of the oceanic lithosphere on which the volcanic islands are built. This physical variable is best constrained because of our fundamental understanding that oceanic lithosphere thickening results from thermal contraction or conductive heat loss as it ages away from the ridge (e.g., Parsons and Sclater, 1977; Stein and Stein, 1992; Phipps Morgan and Smith, 1992). If we then assume intra-plate magma generation occurs in the sub-lithospheric mantle by decompression melting, then the geochemical signatures of OIB erupted on older, thickened lithosphere should be characterized by high mean pressure and low mean extent of melting, whereas OIB erupted on younger, thin lithosphere should be characterized by low mean pressure and high mean extent of melting as illustrated in Fig. 1. This concept was inspired by the recognition of the effect of sub-ridge lithosphere thickness variation on MORB chemistry (Niu and Hékinian, 1997; Niu and O'Hara, 2008) and encouraged by the pioneering work of Ellam (1992) and Haase (1996) on OIB. Thanks to the availability of the large GEOROC database (http://georoc.mpch-mainz.gwdg.de/georoc/) compiled by the MPI GEOROC data team, we are now able to further test this concept.

3. Data and treatment

3.1. OIB geochemical data

The geochemical data we used are exclusively from the GEOROC database. These include mostly bulk-rock analyses and some glass analyses for major and trace elements of over 20,000 samples ranging in composition from highly evolved andesites/basaltic andesites (minor), to tholeiitic basalts (abundant), to alkali rich basalts (relatively abundant) and to rocks highly enriched in alkalis such as basanite or rarely nephelinite (minor) from 189 ocean islands in the Pacific (108 islands), Atlantic (56 islands) and Indian (25 islands) ocean basins (Fig. 2, only island groups are shown). We excluded samples with SiO_2>53 wt.% to ensure we examine mantle melts with minimal crustal level modification. This consideration and the age data constraint (see below) leave us with 115 islands and 12,996 samples to work with.

3.1.1. Correction for fractionation effect to $Mg^{\#}=0.72$

To reveal major element signals of mantle (vs. crustal level) processes, we further corrected for fractionation effect to $Mg^{\#}=0.72$ (see Niu et al., 1999, 2002; Niu and O'Hara, 2008) because basaltic melts with $Mg^{\#}>0.72$ are in equilibrium with mantle olivine of Fo>89.6 (Roeder and Emslie, 1970; Niu and O'Hara, 2008). The database has fewer samples with trace element analyses and the quality is generally poor because analytical errors differ between methods and between laboratories. However, for rare earth elements (REEs), the quality of an individual REE is constrained by normalized REE "patterns". For this reason, we used REEs such as La, Sm and Yb if available. In our discussion, we use La/Sm and Sm/Yb ratios as they are essentially unaffected by crystallization (i.e., no need to correct for this effect).

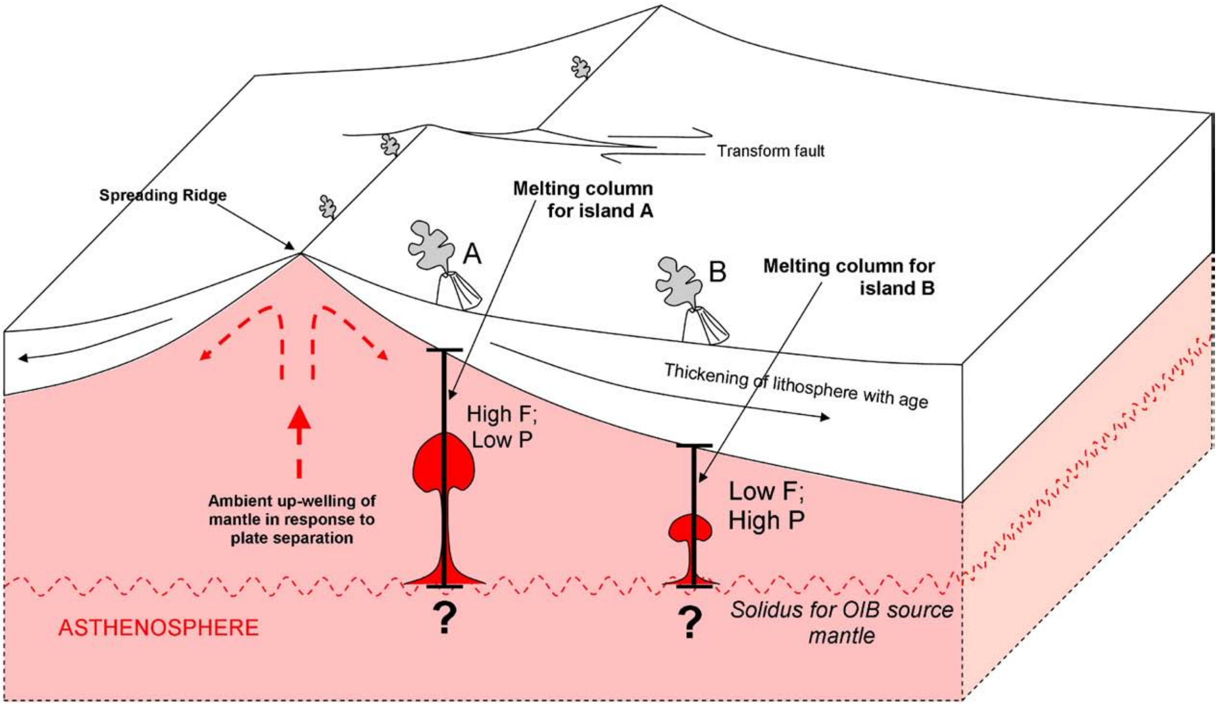

Fig. 1. Schematic diagram illustrating the concept of lithosphere thickness control on the composition of ocean island basalts (OIB). If the island (Island A) is located on the younger and thinner lithosphere, the sub-lithospheric melting column will be tall, allowing great extent of decompression melting (high F) with the melt having low pressure signature (low P). If the island (Island B) is built on the older and thicker lithosphere, the sub-lithospheric melting column will be short, resulting in low extent of decompression melting (low F) with the melt having high pressure signature (high P).

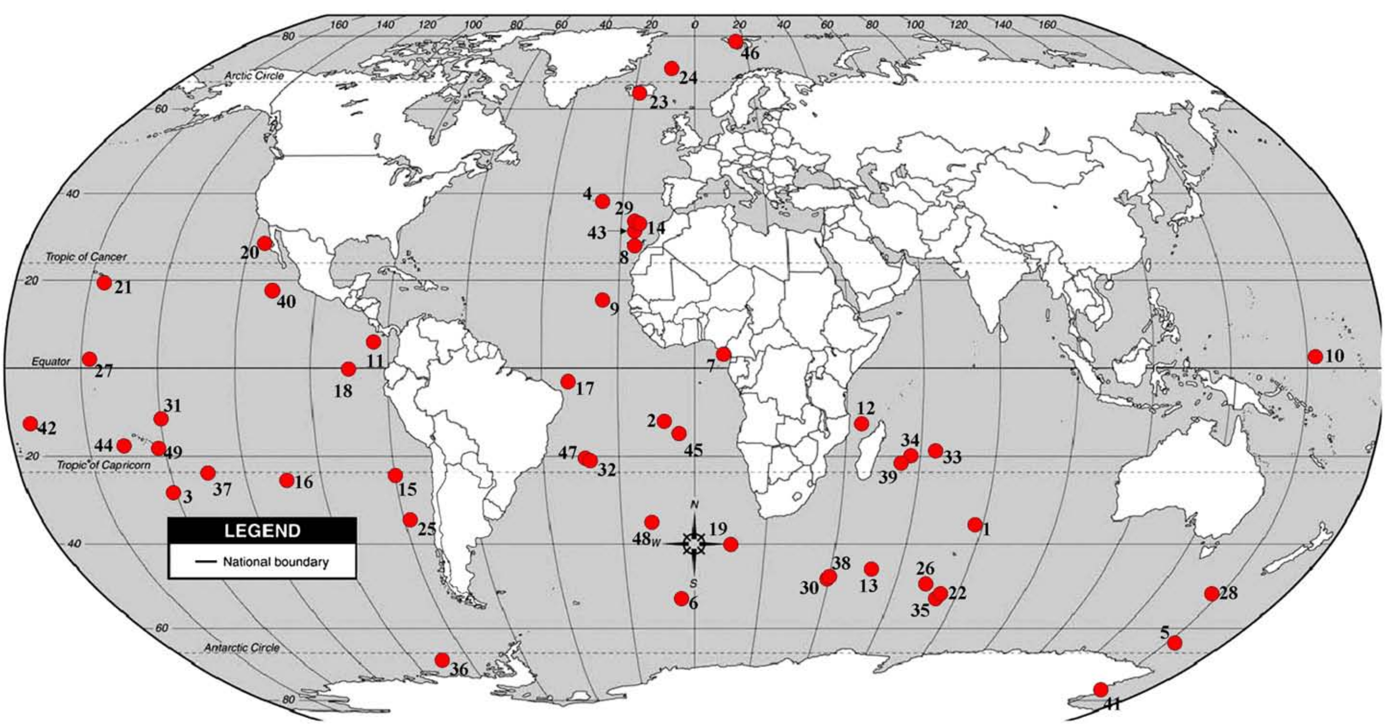

Fig. 2. Island groups: 1, Amsterdam–St. Paul (2); 2, Ascension (1); 3, Austral-Cook (12); 4, Azores (10); 5, Balleny (2); 6, Bouvet (1); 7, Cameroon Line (5); 8, Canary Islands (8); 9, Cape Verde (10); 10, Caroline (10); 11, Cocos (1); 12, Comoros (5); 13, Crozet (4); 14, Desertas (3); 15, Desventuradas (3); 16, Easter seamount (1); 17, Fernando de noronha (1); 18, Galapagos (23); 19, Gough chain (1); 20, Guadalupe (1); 21, Hawaiian (12); 22, Heard (1); 23, Iceland (4); 24, Jan Mayen (1); 25, Juan Fernandez (3); 26, Kerguelen (7); 27, Line Island Chain (1); 28, Macquarie (1); 29, Maderia (2); 30, Marion (1); 31, Marquesas (12); 32, Martin Vas (1); 33, Mascarene (1); 34, Mauritius (1); 35, Mcdonald (1); 36, Peter I island (1); 37, Pitcairn, Gambier (6); 38, Prince Edward (1); 39, Reunion (1); 40, Revillagigedo (4); 41, Ross Island (1); 42, Samoan (4); 43, Selvagen (2); 44, Society (10); 45, St Helena (1); 46, Svalbard (1); 47, Trinidade (1); 48, Tristan da Cunha (5); 49, Tuamotu (1). On diagram; island chains marked with red circle and number. Islands chains given in alphabetical order and number of islands associated with that chain in brackets. Map courtesy of http://chuma.cas.usf.edu/~juster/volc1/world%20map.gif. (For interpretation of the references to colour in this figure legend, the reader is referred to the web version of this article.)

Correction of the major element composition for fractionation effect to $Mg^{\#} = 0.72$ is relatively straightforward both in concept and in practice for MORB (see Niu et al., 1999; Niu and O'Hara, 2008) because the global MORB data are electron probe analyses of glasses (quenched melts) (PETDB: www.petdb.org) with inter-laboratory discrepancies (if any) readily reconciled (see Niu and Batiza, 1997; Lehnert et al., 2000). A general set of liquid lines of descent (LLDs) can also be readily derived from these melt compositions. In contrast, most of the OIB data (http://georoc.mpch-mainz.gwdg.de/georoc/) are whole-rock analyses (i.e., not melts) and vary significantly in composition within a given lava suite, between suites, between islands and between island groups. It is therefore very difficult to derive a general set of LLDs for fractionation correction. Because both OIB and MORB are evolved from mantle melts with olivine, spinel, plagioclase and clinopyroxene as common liquidus phases during their cooling-induced crystallization, we assume that the general set of LLDs derived from MORB melts (Niu et al., 1999; Niu and O'Hara, 2008; also see Appendix A) applicable to the global OIB data set. We thus corrected the 12996 global OIB (<53 wt.% SiO_2; including the alkalic varieties) samples from the 115 islands for fractionation effect to $Mg^{\#} = 0.72$. This correction is adequately effective (e.g., for 115 island averages, the total is $99.4 \pm 1.21\%$) and the correction-associated errors do not affect the interpretations because these errors are significantly smaller than the range of compositional variation and should be averaged out in the island-averaged compositions we use to interpret the processes. The island-averaged data after the correction are presented in Table 2 and plotted as a function of lithosphere thickness in Fig. 3 (the left column under "MORB LLD Corrected").

While our assumption in applying MORB LLDs to correct OIB for fractionation effect is reasonable, it is preferable if the data correction can be verified. As discussed above, it is unrealistic to derive LLDs from individual OIB suites based on bulk-rock analyses (i.e., "mechanical mixtures" of melt and minerals vs. melt like MORB data), and it is further problematic to obtain a general set of LLDs applicable to the global OIB database. We have, however, located the data from Kilauea Iki Lava Lake of Hawaii (see Wright and Fiske, 1971; Helz, 1987), which provide an excellent set of LLDs. Compositionally, these Kilauea lavas are typical OIB with "medium-K" ($K_2O = \sim 0.4$ to 1.1 wt.%; see Le Maitre, 1989) relative to MORB that are K-poor ($K_2O < 0.2$ wt.%). Details of the LLDs and correction procedure are given in Appendix A. The island-averaged OIB data after fractionation correction using the Kilauea LLDs are plotted as a function of lithosphere thickness in Fig. 3 (the right columns under "OIB LLD Corrected") to compare with MORB LLD-corrected data. Island-averaged data points using the two different LLD corrections are not identical, but the variation as a function of the lithosphere thickness is remarkably similar as expected.

The primitive Kilauea OIB have lower SiO_2, Al_2O_3 and CaO, but higher FeO and TiO_2 than primitive MORB at a given MgO (e.g., ~10 wt.%). This is to a first-order consistent with higher pressure and lower extent of melting beneath the thickened lithosphere in the case of Hawaii than beneath ocean ridges. If MORB represent melts erupted on lithosphere with "zero" thickness, then the Hawaiian lavas represent OIB erupted on lithosphere of full thickness (>70 Ma, and hence ≥90 km thick). They thus represent the two "end-member" scenarios when accounting for the influence of lithosphere thickness. Thus, if LLDs for individual islands could be determined and used for correction to $Mg^{\#} = 0.72$, the LLD data would plot between MORB and OIB LLD values. That is, the trends in Fig. 3 are significant by using whatever reasonable basaltic LLDs.

3.1.2. Data averaging

Niu and O'Hara (2009-this issue) have discussed the *pros and cons* of averaging rock compositional data. The principle is straightforward, and it is the research objectives and scientific questions to be addressed that determine whether it is necessary to average the data. For example, if the objective is to understand the petrogenesis of a suite of rocks and to test if individual samples of the suite may (or may not) be genetically related, then averaging must be avoided. Furthermore, Niu and O'Hara (2009-this issue) demonstrate for the first time that primitive MORB melts possess excess Eu and Sr, which is an important "discovery", but has been concealed in the averaging of MORB compositions. Conversely, compositional averaging is a powerful way to reveal first-order MORB compositional systematics as a function of ridge separation rate (Niu and Hékinian, 1997; Rubin and Sinton, 2007) or ridge axial depth (Klein and Langmuir, 1987; Niu and O'Hara, 2008), and to distinguish MORB from mantle melts from other tectonic settings such as OIB and IAB (Hofmann, 1988; Sun and McDonough, 1989; Pearce and Peate, 1995; Niu and O'Hara, 2003). Our objective here is not to focus on a particular suite of OIB samples on a given island, but rather to investigate whether first-order OIB compositional systematics vary as a function of lithosphere thickness on a global scale. Therefore, it is necessary to average out compositional details that are important only on local scales (e.g., between-sample comparisons within a given OIB suite or on a given island).

Our strategy is to average all the available lava compositional data from each volcanic island so as to compare between island differences as a function of lithosphere thickness. However, one may question whether such averaging is appropriate due to the variety of compositions on a single island. The Hawaiian Islands show significant compositional variation from the shield stage (tholeiite with minor alkalic basalts) to the post-shield stage (tholeiitic and alkalic basalts), and to the post-erosional stage (alkalic basalts, including nephelinite basalt and basanitoids) (see Macdonald and Katsura, 1964) over a period of ~2–2.5 m.y. (Doell and Dalrymple, 1973). Our methods do result in the averaging of these data from individual islands, but this is important for our objective. For example, when examining the effect of spreading rate variation on MORB chemistry, we must average MORB data with respect to spreading rate within the chosen spreading rate windows (regardless of chemical variability and geographic location; see Niu and Hékinian, 1997; Rubin and Sinton, 2007). To examine if MORB chemistry varies with ridge depth, we must average the MORB data with respect to ridge depth within chosen depth intervals (regardless of chemical variability and geographic location; see Niu and O'Hara, 2008). In order to examine the effect of the lithosphere thickness control on OIB chemistry only, we need to average the global OIB data with respect to chosen lithosphere thickness intervals (regardless of chemical variability and geographic location; see Niu and Humphreys, 2008).

Furthermore, (1) we focus on the bulk response of the entire island-building volcanism to the potential control of lithosphere thickness during island-building magmatism (i.e., ~2–2.5 m.y) where lithosphere thickness is essentially constant; (2) despite within-island compositional variation (tholeiitic to alkalic), the lavas form a compositional continuum, and it is subjective to arbitrarily divide these rocks as different entities without yet understanding their origin (e.g., Batiza, 1980; Frey and Rhodes, 1993; Fekiacova et al., 2007; Konter et al., 2009); (3) different volcanoes on the same island (e.g., the "Kea" and "Loa" volcanoes on Hawaiian islands from Oahu, to Maui and to Hawai i) differ in major and trace element abundances and radiogenic isotopes (e.g., Frey and Rhodes, 1993; Fekiacova et al., 2007), and in this study there is no logically sound basis to treat these coeval volcanoes differently as their difference is not caused by lithosphere thickness difference; (4) the fact that alkalic basalts (including the rare basanite and nephelinite) erupt on islands of thickened lithosphere but are rare/absent on islands of thin lithosphere including ocean ridges and near-ridge seamounts indicate that these differences are controlled by physical processes that are directly or indirectly related to lithosphere thickness. Therefore, to average all the existing data of compositionally varying lavas from a given island regardless of chemical variation is an objective and logically sound

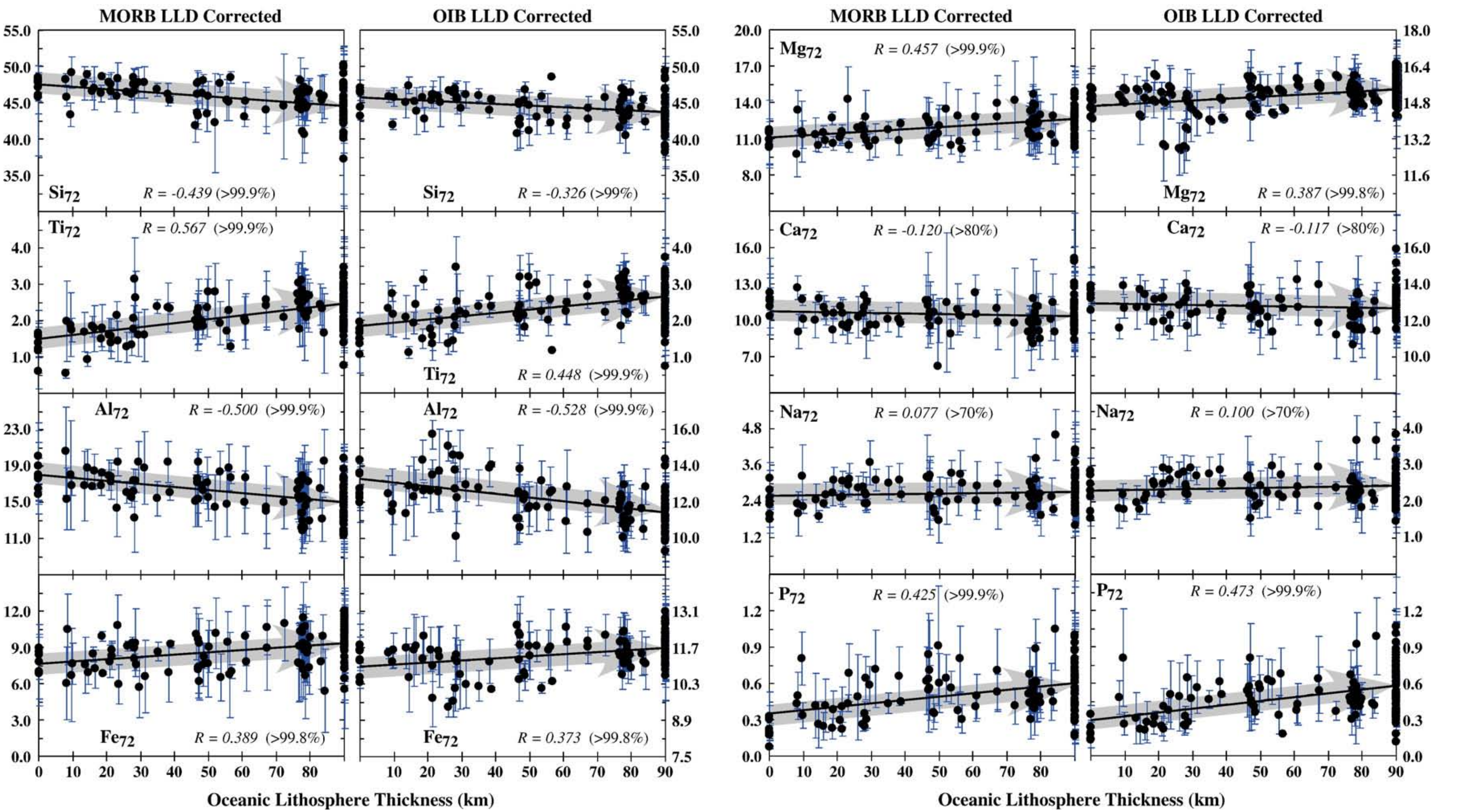

Fig. 3. Island-averaged major element data corrected for fractionation effect to $Mg^{\#} = 0.72$ plotted as a function of the lithosphere thickness. Each data point represents average composition for a given volcanic island; error bars represent 2 standard deviations from the mean (see Tables 1 and 2 for data). The averaged data points define trends that are consistent with increasing mean pressure and decreasing mean extent of melting from beneath thin lithosphere to beneath thick lithosphere (see text for details). Plotted in left panels are data corrected using liquid lines of descent (LLDs) derived from MORB (see Niu and O'Hara, 2008) and plotted in right panels are data corrected using LLDs derived from Kilauea Iki lava lake data (Wright and Fiske, 1971; Helz, 1987) (see Appendix A for details). The data corrected using the two different sets of LLDs differ in detail, but the island-averaged OIB trends as a function of lithosphere thickness variation remain the same.

Table 1
Basic data of ocean Islands studied.

Island	Ocean	Location (latitude, longitude)	Volcano age (Myr)	Ref.	Lithosphere age (Myr)	Δ Age (Myr)	Lithosphere thickness (km)
Ascension	Atlantic	(−7.93, −14.37)	1.50	[6]	6.08	4.58	23.53
Bioko	Atlantic	(3.40,8.70)	30.00	[3]	149.47	119.47	90.00
Boa Vista	Atlantic	(16.10, −23.00)	50.00	[13]	188.97	138.97	90.00
Chao	Atlantic	(32.50, −16.50)	3.60	[25]	148.45	144.85	90.00
Deserta grande	Atlantic	(32.51, −16.50)	3.60	[25]	148.78	145.18	90.00
Faial	Atlantic	(38.58, −28.70)	0.73	[14]	7.99	7.26	29.63
Fernando poo	Atlantic	(3.80,8.24)	30.00	[3]	149.47	119.47	90.00
Flores	Atlantic	(39.22, −31.22)	2.20	[1]	10.26	8.06	31.23
Fogo	Atlantic	(14.90, −24.35)	5.00	[6] [13]	175.82	170.82	90.00
Fuerteventura	Atlantic	(29.00, −14.00)	20.60	[13]	192.11	171.51	90.00
Gough	Atlantic	(−40.32, −9.92)	1.00	[13]	50.22	49.22	77.17
Graciosa	Atlantic	(39.05, −28.05)	0.62	[14]	12.98	12.36	38.67
Gran Canaria	Atlantic	(28.00, −15.50)	14.50	[6] [7] [8]	192.60	178.10	90.00
Hierro	Atlantic	(27.80, −18.00)	1.12	[7] [8]	170.08	168.96	90.00
Iceland	Atlantic	(63.90, −19.60)	16.00	[13]	0.00	0.00	0.00
Inaccessible	Atlantic	(−37.32, −12.73)	0.30	[13]	23.99	23.69	53.54
Jan Mayen	Atlantic	(71.00, −8.50)	5.00	[18]	23.13	18.13	46.84
Kolbeinsey	Atlantic	(67.13, −18.60)	16.00	[13]	0.00	0.00	0.00
La Gomera	Atlantic	(28.10, −17.20)	12.00	[7] [8]	179.05	167.05	90.00
La Palma	Atlantic	(28.50, −18.00)	1.77	[6] [7] [8]	171.20	169.43	90.00
Lanzarote	Atlantic	(29.20, −13.50)	15.50	[7] [8]	186.71	171.21	90.00
Maderia	Atlantic	(32.76, −16.81)	4.60	[16]	145.95	141.35	90.00
Maio	Atlantic	(15.15, −23.20)	30.00	[13]	193.95	163.95	90.00
Pagalu	Atlantic	(−1.26, 5.37)	30.00	[3]	114.79	84.79	90.00
Pico	Atlantic	(38.47, −28.30)	0.30	[15]	10.38	10.08	34.92
Porto Santo	Atlantic	(33.08, −16.03)	14.30	[16]	150.04	135.74	90.00
Principe	Atlantic	(1.62,7.45)	30.00	[19]	134.70	104.70	90.00
Sal	Atlantic	(16.70, −23.00)	60.00	[13]	186.62	126.62	90.00
Santiago	Atlantic	(14.90, −24.30)	30.00	[13]	190.60	160.60	90.00
Sao Jorge	Atlantic	(38.67, −28.05)	0.55	[14]	12.59	12.04	38.16
Sao Miguel	Atlantic	(37.80, −25.50)	26.50	[6] [13]	47.12	20.62	49.95
Sao Tome	Atlantic	(0.42,6.58)	30.00	[3]	129.72	99.72	90.00
St Helena	Atlantic	(−15.95, −5.70)	14.60	[13]	45.45	30.85	61.10
Tenerife	Atlantic	(28.30, −16.60)	11.60	[6] [7] [8]	182.54	170.94	90.00
Terceira	Atlantic	(27.22, −38.72)	0.40	[5] [6]	18.64	18.24	46.98
Trinidade	Atlantic	(−20.50, −29.30)	3.40	[6] [17]	102.19	98.79	90.00
Tristan da cuhna	Atlantic	(−37.05, −12.30)	0.21	[13]	26.20	25.99	56.08
Vestmannaeyjar islands	Atlantic	(63.48, −20.18)	0.00	[13]	0.00	0.00	0.00
Amsterdam	Indian	(−37.83,77.55)	3.00	[6]	4.72	1.72	14.41
Foch	Indian	(−49.75,68.50)	34.00	[6] [21]	34.80	0.80	9.86
Heard	Indian	(−53.00,73.30)	40.00	[11]	46.69	6.69	28.45
Ile aux Cochon	Indian	(−46.20, 50.70)	1.00	[28]	143.22	142.22	90.00
Ile de la Possession	Indian	(−46.40, 51.70)	8.00	[28]	166.04	158.04	90.00
Ile de L'ouest	Indian	(−46.50, 52.15)	9.00	[28]	183.29	174.29	90.00
Ile de L'ouest	Indian	(−49.75, 68.50)	33.00	[6] [21]	34.50	1.50	13.48
Kerguelen	Indian	(−49.75, 68.50)	34.00	[6] [21]	34.57	0.57	8.31
Mauritius	Indian	(−20.43, 57.64)	7.80	[6]	56.74	48.94	76.95
Reunion	Indian	(−21.25, 55.75)	2.00	[6]	70.06	68.06	90.00
Aitutaki	Pacific	(−18.87–159.77)	8.43	[2] [10]	59.26	50.83	78.43
Atiu	Pacific	(−19.98, −158.10)	8.58	[2] [10]	60.33	51.75	79.13
Baltra	Pacific	(−0.41, −90.22)	2.80	[13]	4.91	2.11	15.99
Bora Bora	Pacific	(−16.46, −151.74)	6.08	[4] [10]	56.21	50.13	77.88
Darwin	Pacific	(1.65, −92.00)	2.10	[13]	1.83	0.00	0.00
Easter Island	Pacific	(−27.17, −109.33)	2.54	[6] [13]	4.81	2.27	16.57
Eiao	Pacific	(−8.00, −140.67)	6.03	[10]	62.92	56.89	82.97
Espanola	Pacific	(−1.38, −89.67)	2.30	[6] [13]	7.93	5.63	26.10
Fangatufa	Pacific	(−22.29, −138.54)	12.95	[10]	32.16	19.21	48.21
Fatu hiva	Pacific	(−10.54, −138.85)	3.72	[6] [10]	52.33	48.61	76.69
Fatu huku	Pacific	(−9.42, −138.92)	2.65	[10] [17]	52.37	49.72	77.56
Fernandina	Pacific	(−0.34, −91.47)	2.10	[13]	8.86	6.76	28.61
Floreana	Pacific	(0.23, −90.42)	1.90	[13]	8.14	6.24	27.48
Gambier Islands	Pacific	(−23.17, −135.00)	6.20	[10] [17]	25.64	19.44	48.50
Gardner Pinnacle	Pacific	(25.00, −167.98)	12.30	[6] [20]	124.21	111.91	90.00
Genovesa	Pacific	(0.30, −89.91)	2.80	[13]	1.99	0.00	0.00
Hatutu	Pacific	(−7.93, −140.55)	4.90	[10]	62.69	57.79	83.62
Hawaii	Pacific	(20.23, −155.80)	0.43	[6] [10] [20]	112.19	111.76	90.00
Hiva oa	Pacific	(−9.75, −139.00)	4.26	[6] [10]	52.61	48.35	76.49
Huahine	Pacific	(−16.75, −151.00)	4.99	[9] [10]	55.15	50.16	77.91
Isabela	Pacific	(−0.41, −91.03)	1.90	[6] [13]	8.35	6.45	27.94
Isla Isabela	Pacific	(−0.90, −91.00)	1.90	[6] [13]	8.35	6.45	27.94
Kahoolawe	Pacific	(20.54, −156.55)	1.03	[6] [10] [20]	111.74	110.71	90.00
Kauai	Pacific	(22.0, −159.50)	5.10	[6] [10] [20]	114.08	108.98	90.00
La Perouse Pinnacle	Pacific	(23.82, −167.97)	12.00	[6] [10] [20]	124.72	112.72	90.00
Lanai	Pacific	(20.88, −156.88)	1.28	[6] [10] [20]	112.27	110.99	90.00

(continued on next page)

Table 1 (*continued*)

Island	Ocean	Location (latitude, longitude)	Volcano age (Myr)	Ref.	Lithosphere age (Myr)	Δ Age (Myr)	Lithosphere thickness (km)
Macquarie Island	Pacific	(−54.48, 158.97)	11.50	[22]	37.96	26.46	56.58
Mangaia	Pacific	(−21.93, −157.93)	21.90	[2] [10]	52.42	30.52	60.77
Marchena	Pacific	(0.35, −90.40)	2.50	[13]	2.33	0.00	0.00
Mas a Tierra	Pacific	(−33.50, −78.50)	4.23	[17]	41.57	37.34	67.22
Mas Afuera	Pacific	(−33.50, −78.50)	2.44	[17]	45.72	43.28	72.37
Matotiri	Pacific	(−28.33, −143.54)	31.95	[2] [10]	32.70	0.75	9.51
Maui	Pacific	(20.91, −156.59)	1.32	[20]	110.67	109.35	90.00
Mehetia	Pacific	(−17.92, −148.03)	0.55	[6] [9]	50.08	49.53	77.41
Molokai	Pacific	(21.18, −157.77)	1.90	[6] [10] [20]	112.10	110.20	90.00
Motane	Pacific	(−10.00, −138.85)	2.26	[10] [17]	52.33	50.07	77.83
Motu nao	Pacific	(−10.40, −138.54)	1.27	[6] [10]	51.93	50.66	78.30
Mururoa atoll	Pacific	(−21.83, −138.88)	11.58	[10]	32.04	20.46	49.75
Nihoa	Pacific	(23.05, −161.92)	7.20	[6] [10] [20]	117.48	110.28	90.00
Niihau	Pacific	(21.83, −160.18)	4.89	[6] [20]	115.74	110.85	90.00
Nuku hiva	Pacific	(−8.93, −140.00)	5.30	[6] [10]	57.48	52.18	79.46
Oahu	Pacific	(21.43, −158.18)	2.60	[10] [20]	112.57	109.97	90.00
Pinta	Pacific	(0.63, −90.72)	2.10	[13]	1.44	0.00	0.00
Pinzon	Pacific	(−0.70, −90.70)	2.30	[13]	5.90	3.60	20.87
Pitcairn	Pacific	(−25.07, −130.10)	0.95	[6] [10]	19.39	18.44	47.24
Rabida	Pacific	(−0.40, −90.67)	2.30	[13]	5.22	2.92	18.80
Raiatea	Pacific	(−16.92, −151.35)	5.60	[4] [10]	55.74	50.14	77.89
Raivavae	Pacific	(−23.85, −147.63)	7.57	[2] [10]	33.01	25.44	55.48
Rapa	Pacific	(−27.58, −144.33)	5.20	[2] [10]	27.67	22.47	52.15
Rarotonga	Pacific	(−21.25, −159.75)	3.64	[2] [10]	40.93	37.29	67.18
Rimatara	Pacific	(−22.67, −152.75)	15.00	[2] [10]	33.43	18.43	47.23
Roca Redonda	Pacific	(0.30, −91.52)	2.30	[13]	6.69	4.39	23.04
Ross Island	Pacific	(−77.67, 168.00)	1.30	[12]	59.73	58.43	84.08
Rututu	Pacific	(−22.42, −151.33)	12.98	[2] [10]	31.11	18.13	46.83
San Cristobal	Pacific	(−0.92, −89.40)	2.30	[6] [13]	6.10	3.80	21.44
Santa Cruz	Pacific	(−0.49, −90.26)	2.80	[6] [13]	5.62	2.82	18.48
Santa Fe	Pacific	(−0.85, −90.50)	2.30	[13]	6.07	3.77	21.37
Savaii	Pacific	(−13.50, −172.50)	4.99	[23]	115.11	110.12	90.00
Tahaa	Pacific	(−16.50, −151.50)	3.20	[9] [10]	55.86	52.66	79.82
Tahiti	Pacific	(−17.70, −149.45)	0.80	[4] [6]	52.05	51.25	78.75
Tahuata	Pacific	(−9.97, −139.08)	2.40	[6] [10]	52.72	50.32	78.03
Tubuai	Pacific	(−23.38, −149.45)	10.60	[2] [10]	28.30	17.70	46.28
Tutuila	Pacific	(−14.30, −170.70)	1.40	[10]	112.35	110.95	90.00
Ua Huka	Pacific	(−8.92, −139.53)	4.80	[6] [10]	56.58	51.78	79.15
Ua pou	Pacific	(−9.42, −140.00)	5.61	[10]	54.18	48.57	76.66
Upolu	Pacific	(− 14.00, −171.70)	2.80	[10]	114.02	111.22	90.00
Wolf	Pacific	(1.38, −91.81)	2.10	[6] [13]	2.63	0.53	8.01

References: [1] Azevedo and Ferreria, 2006; [2] Bonneville, 2002; [3] Burke, 2001; [4] Calmant and Cazenave, 1986; [5] Calvert et al., 2006; [6] Caplan-Auerbach et al., 2000; [7] Carracedo et al., 1998; [8] Carracedo et al., 2002; [9] Clouard and Bonneville, 2004a; [10] Clouard and Bonneville, 2004b; [11] Coffin et al., 2002; [12] Esser et al., 2004; [13] Faure, 2001; [14] Feraud et al., 1980 [15] Franca et al., 2006; [16] Geldmacher et al., 2005; [17] Gripp and Gordon, 2002; [18] Haase et al., 1996; [19] Halliday et al., 1988; [20] http://www.soest.hawaii.edu/GG/HCV/haw_formation.htm; [21] Ingle et al., 2003; [22] Kamenetsky et al., 2000; [23] Koppers et al., 2008; [24] Plesner et al., 2002; [25] Schwartz et al., 2004; [26] Storevedt et al., 1989; [27] Haase et al., 2000; [28] Recq et al., 1998.

approach in order to evaluate the effect of lithosphere thickness variation (vs. source effects and other factors) on a global scale. The island-averaged data are given in Tables 2 and 3.

3.2. Thickness of the oceanic lithosphere

The thickness of the oceanic lithosphere at the time of OIB volcanism is determined from the age of the lithosphere at that time using the half-space lithosphere cooling model, i.e., $T=11*t^{1/2}$ (where T is lithosphere thickness in km, and t is age in Ma). The model is reliable for lithosphere younger than ~70 Myrs (Parsons and Sclater, 1977; Phipps Morgan and Smith, 1992; Stein and Stein, 1992). Because oceanic lithosphere reaches its full thickness at the age of ~70 Myrs, we assume a constant thickness of ~90 km (i.e., $11*70^{1/2}=92$ km) for older lithosphere. The base of the lithosphere we consider would approximate the ~1250 °C isotherm of Parsons and Sclater (1977), and is consistent with a mantle potential temperature of 1315 °C (McKenzie et al., 2005). The plate model (Stein and Stein, 1992) gives an isotherm of 1450 °C at the base of the lithosphere, which may be too hot (see McKenzie et al., 2005). In any case, the choice of lithosphere definition (Anderson, 1995) or isotherm values at the base of the chosen lithosphere does not affect our conclusions as the calculations are consistent for all volcanic islands. Although the age of the oceanic lithosphere is reasonably well constrained (see Muller et al., 1997) and the age of a volcanic island can be dated, the seafloor magnetic anomalies do not always provide lithosphere ages with adequate resolution for this study. Therefore, for consistency, all lithosphere ages beneath individual volcanic islands were calculated (1) using the distance from the island to the corresponding spreading centre along the absolute plate motion direction (DeMets et al., 1990), (2) using the present-day spreading rate (half-rate; using http://ofgs.ori.utokyo.ac.jp/~okino/calc.html, ; DeMets et al., 1990; DeMets et al., 1994), and (3) assuming a constant spreading rate over the past 70 million years. An estimated error of ~10% is insignificant for this study given the large OIB compositional variability on a given volcanic island. Volcanic islands, for which the age of the lithosphere could not be determined, are discarded. Ages for individual volcanic islands are taken from the literature. Volcanic islands for which no age data exist are also discarded. This leaves 115 volcanic islands with adequate geochemical data as well as age information (Table 1).

The age of the volcanic island is subtracted from the age of the lithosphere to give the age of the lithosphere at the time of OIB eruption (ΔAge), from which the thickness of the lithosphere was calculated. Table 1 gives the ages of volcanic islands from the literature, the calculated ages of the corresponding lithosphere, the age difference between the volcanism and the lithosphere as well as calculated thickness of the lithosphere <~70 Ma and assigned 90 km

Table 2
Average compositions of ocean island basalts corrected for fractionation effect to Mg# = ~0.72.

Island	Ocean	N	Si_{72}	Si_{72} σ	Ti_{72}	Ti_{72} σ	Al_{72}	Al_{72} σ	Fe_{72}	Fe_{72} σ	Mn_{72}	Mn_{72} σ	Mg_{72}	Mg_{72} σ	Ca_{72}	Ca_{72} σ	Na_{72}	Na_{72} σ	K_{72}	K_{72} σ	P_{72}	P_{72} σ
Ascension	Atlantic	23	48.38	2.18	1.42	0.56	19.43	1.52	5.95	1.61	0.11	0.04	10.41	0.56	9.79	0.84	3.14	0.50	1.36	0.57	0.66	0.24
Bioko	Atlantic	1	43.37	0.00	3.24	0.00	11.55	0.00	11.03	0.00	0.16	0.00	13.79	0.00	11.52	0.00	2.38	0.00	1.13	0.00	0.59	0.00
Boa Vista	Atlantic	4	41.01	2.96	3.17	0.39	11.37	1.59	11.49	1.33	0.18	0.02	14.77	1.72	11.03	2.65	1.99	0.20	1.05	0.04	0.71	0.42
Chao	Atlantic	19	44.72	1.18	1.97	0.57	16.64	3.06	9.07	2.29	0.12	0.03	12.29	1.48	10.54	0.89	2.49	0.53	0.77	0.22	0.50	0.16
Deserta grande	Atlantic	19	44.45	0.88	2.32	0.19	14.94	2.37	10.47	1.24	0.14	0.02	13.12	1.41	10.41	0.87	2.24	0.25	0.71	0.13	0.43	0.09
Faial	Atlantic	47	47.78	2.07	1.60	0.61	19.42	2.33	5.65	2.46	0.11	0.07	10.33	1.10	9.57	1.25	3.67	0.73	1.62	0.43	0.56	0.16
Fernando poo	Atlantic	16	45.91	1.26	2.22	0.35	13.00	2.61	10.90	1.39	0.18	0.12	13.47	1.50	9.62	1.86	2.33	0.56	1.52	0.53	0.63	0.43
Flores	Atlantic	4	47.86	2.18	1.59	0.72	18.78	4.02	6.57	3.03	0.14	0.01	10.85	1.37	9.58	0.91	3.11	0.36	2.01	0.45	0.69	0.32
Fogo	Atlantic	21	40.94	1.45	2.96	0.34	16.61	1.80	8.94	1.52	0.14	0.02	11.73	1.01	12.74	1.35	3.27	0.56	2.22	0.61	0.85	0.31
Fuerteventura	Atlantic	126	43.41	2.50	2.61	0.72	14.08	2.35	9.93	2.22	0.13	0.03	13.03	1.72	9.81	1.25	2.84	0.59	1.30	0.70	0.64	0.24
Gough	Atlantic	50	48.07	3.09	2.32	0.60	16.80	3.01	7.58	2.70	0.09	0.04	11.29	1.73	8.48	2.61	2.86	0.44	2.36	0.67	0.52	0.20
Graciosa	Atlantic	2	45.45	0.48	2.33	0.17	16.13	0.86	9.22	0.30	0.14	0.01	12.19	0.39	9.76	0.34	2.62	0.24	0.88	0.08	0.43	0.01
Gran Canaria	Atlantic	411	44.36	3.49	3.00	1.02	13.79	3.81	9.08	3.21	0.14	0.07	12.53	2.31	9.52	2.12	2.95	1.23	1.43	1.06	0.66	0.35
Hierro	Atlantic	88	43.39	2.75	2.88	0.92	15.26	3.45	10.03	2.94	0.16	0.05	13.03	2.41	9.93	1.36	3.21	0.85	1.34	0.47	0.86	0.24
Iceland	Atlantic	1974	47.97	2.18	1.23	0.70	16.51	1.32	8.91	1.13	0.16	0.56	11.69	0.70	11.77	1.71	1.97	0.43	0.26	0.33	0.18	0.15
Inaccessible	Atlantic	23	47.74	1.22	1.92	0.60	18.36	2.21	6.49	1.95	0.08	0.04	10.46	0.77	8.86	1.19	3.31	0.44	2.02	0.36	0.54	0.13
Jan Mayen	Atlantic	116	46.21	3.28	1.80	0.63	17.18	3.34	7.31	2.11	0.13	0.03	10.92	0.97	11.66	3.90	2.55	0.50	1.97	0.56	0.61	0.26
Kolbeinsey	Atlantic	2	45.79	0.55	1.15	0.08	15.91	1.14	8.36	0.61	0.17	0.01	10.90	0.59	11.14	0.53	1.81	0.45	0.45	0.01	0.15	0.01
La Gomera	Atlantic	26	47.27	3.54	1.93	1.23	18.67	2.71	5.53	3.22	0.14	0.04	10.25	1.60	9.18	2.14	3.97	0.97	1.81	0.58	0.78	0.25
La Palma	Atlantic	121	43.71	2.84	2.65	0.64	15.97	2.53	8.99	2.64	0.14	0.03	12.07	1.66	10.12	1.94	3.41	0.94	1.36	0.63	0.70	0.21
Lanzarote	Atlantic	155	44.90	2.76	2.34	0.41	13.26	1.41	10.34	1.01	0.14	0.03	13.43	1.00	9.65	1.42	3.00	0.34	1.00	0.28	0.64	0.25
Maderia	Atlantic	193	43.97	2.28	2.29	0.61	15.67	2.64	9.52	2.20	0.16	0.05	12.69	1.56	10.04	1.47	2.81	0.71	0.87	0.24	0.60	0.20
Maio	Atlantic	30	42.21	4.78	2.54	1.43	13.87	3.18	9.25	2.38	0.14	0.04	12.45	2.01	13.08	2.99	2.81	0.84	1.22	1.17	0.68	0.49
Pagalu	Atlantic	25	43.05	1.99	2.82	0.42	12.83	2.47	11.66	1.67	0.13	0.04	14.34	1.65	10.08	1.56	2.50	0.37	1.25	0.40	0.77	0.28
Pico	Atlantic	14	46.83	0.83	2.38	0.19	15.40	1.87	8.63	0.76	0.13	0.01	11.71	0.67	10.06	1.03	3.00	0.54	1.08	0.22	0.41	0.09
Porto Santo	Atlantic	12	45.20	1.40	1.98	0.42	17.48	3.52	7.73	2.40	0.13	0.03	11.32	1.52	11.33	1.29	2.38	0.52	0.66	0.12	0.63	0.24
Principe	Atlantic	21	44.32	3.58	1.91	1.07	16.86	3.84	8.16	3.50	0.15	0.12	11.87	1.99	9.96	1.68	3.42	1.59	1.48	0.64	0.75	0.25
Sal	Atlantic	20	37.28	4.83	2.71	0.76	11.79	2.92	11.28	2.55	0.18	0.02	14.68	2.22	15.15	3.66	2.72	0.73	1.19	0.51	0.98	0.40
Santiago	Atlantic	41	42.42	1.62	2.91	0.53	14.51	2.62	10.05	1.74	0.14	0.03	12.94	1.46	11.47	1.37	2.50	0.79	1.19	0.72	0.74	0.33
Sao Jorge	Atlantic	10	46.19	1.54	2.35	0.67	19.42	2.25	6.92	2.42	0.10	0.03	10.83	1.23	10.05	1.41	3.09	0.55	1.35	0.31	0.64	0.25
Sao Miguel	Atlantic	38	45.95	2.07	2.77	0.71	15.52	2.53	9.02	2.16	0.15	0.05	12.07	1.67	9.94	1.83	2.67	0.51	1.77	0.79	0.58	0.24
Sao Tome	Atlantic	21	42.65	2.70	3.46	1.62	14.94	3.31	9.00	2.53	0.13	0.04	12.20	1.55	9.54	1.52	3.70	0.94	1.58	0.66	0.91	0.25
St Helena	Atlantic	71	45.27	2.55	1.97	0.75	17.75	3.44	7.81	2.45	0.12	0.05	11.51	1.49	10.51	1.97	2.90	0.81	1.12	0.38	0.47	0.18
Tenerife	Atlantic	343	45.07	2.81	2.41	0.83	17.78	2.81	7.31	2.94	0.12	0.03	11.08	1.66	10.25	1.82	3.39	1.07	1.58	0.69	0.78	0.29
Terceira	Atlantic	38	47.69	1.75	1.91	0.58	17.62	1.99	7.13	2.34	0.13	0.03	11.02	1.04	10.17	1.49	3.16	0.58	1.10	0.26	0.81	0.34
Trinidade	Atlantic	39	40.45	3.25	2.86	1.43	15.34	3.71	9.38	3.56	0.14	0.04	12.47	2.18	10.88	1.36	4.11	1.28	1.78	1.47	0.96	0.47
Tristan da cuhna	Atlantic	62	45.11	2.55	2.28	0.82	18.84	2.49	6.70	3.51	0.10	0.03	10.75	1.67	10.41	1.37	3.30	0.79	2.61	0.84	0.78	0.27
Vestmannaeyjar islands	Atlantic	41	46.12	2.59	1.56	0.36	18.06	1.82	8.58	1.51	0.15	0.04	11.66	0.93	10.36	1.58	3.17	0.52	0.63	0.25	0.30	0.20
Amsterdam	Indian	24	48.88	0.55	0.91	0.19	18.79	2.06	6.93	1.04	0.10	0.02	10.47	0.59	11.82	0.53	1.89	0.19	0.53	0.07	0.23	0.19
Foch	Indian	28	49.16	2.18	1.72	0.33	16.82	1.04	7.63	1.69	0.12	0.03	11.32	1.15	10.05	0.70	2.22	0.24	0.84	0.37	0.31	0.11
Heard	Indian	68	46.62	2.97	3.15	1.12	13.27	3.73	9.36	2.82	0.13	0.06	12.81	2.14	9.02	2.21	2.62	0.59	2.29	0.74	0.62	0.18
Ile aux Cochon	Indian	1	47.67	0.00	0.75	0.00	19.85	0.00	6.44	0.00	0.11	0.00	10.44	0.00	9.93	0.00	3.17	0.00	1.98	0.00	0.54	0.00
Ile de la Possession	Indian	36	45.08	1.91	2.52	1.72	15.53	3.00	9.09	1.67	0.13	0.02	12.09	1.24	12.10	1.77	2.36	0.57	1.11	0.66	0.41	0.15
Ile de L'est	Indian	44	45.05	2.31	2.29	0.49	13.26	2.29	10.32	1.21	0.14	0.02	13.18	1.25	11.64	2.29	2.21	0.30	0.99	0.24	0.39	0.09
Ile de L'ouest	Indian	253	47.73	2.28	1.68	0.53	16.81	3.83	7.53	2.31	0.13	0.05	11.31	1.39	9.99	1.48	2.45	0.51	1.02	0.80	0.39	0.27
Kerguelen	Indian	6	45.85	1.33	1.97	1.10	15.35	3.41	10.48	2.92	0.13	0.05	13.36	1.63	9.06	1.43	1.97	0.75	1.61	0.48	0.47	0.20
Mauritius	Indian	61	45.66	1.49	1.76	0.49	15.34	2.68	10.27	1.91	0.13	0.03	13.28	1.63	10.01	0.90	2.50	0.38	0.67	0.48	0.28	0.16
Reunion	Indian	541	45.87	5.96	1.93	0.49	15.95	2.60	9.25	2.68	0.16	0.91	12.44	2.51	11.64	3.33	2.35	0.46	0.77	0.38	0.35	0.17
Aitutaki	Pacific	37	40.64	2.56	2.21	0.28	12.19	1.73	10.67	1.05	0.17	0.03	13.72	0.81	10.66	1.17	3.81	0.67	1.42	0.42	0.86	0.25
Atiu	Pacific	20	44.38	1.86	2.09	0.30	15.25	3.95	8.50	2.65	0.13	0.05	12.19	2.39	11.17	0.98	2.48	0.41	1.14	0.32	0.44	0.19
Baltra	Pacific	3	46.67	1.27	1.83	0.28	16.77	0.32	8.42	0.61	0.11	0.03	11.50	0.52	11.04	0.99	2.33	0.12	0.39	0.13	0.22	0.12
Bora Bora	Pacific	6	46.78	1.33	2.49	0.48	13.85	2.73	9.36	1.73	0.11	0.05	12.64	1.57	9.94	1.89	2.22	0.11	1.28	0.37	0.38	0.12
Darwin	Pacific	4	48.53	0.34	1.56	0.42	17.73	1.12	7.78	0.72	0.13	0.03	10.90	0.41	11.79	0.36	2.37	0.24	0.26	0.03	0.20	0.03
Easter Island	Pacific	89	47.02	2.92	1.77	0.63	18.45	1.88	7.18	1.58	0.11	0.05	10.86	0.61	10.57	1.00	2.61	0.41	0.52	0.27	0.39	0.22
Eiao	Pacific	114	46.23	2.55	2.42	0.57	16.51	2.21	7.80	2.30	0.11	0.03	11.35	1.67	10.10	1.83	2.56	0.60	0.90	0.44	0.50	0.24
Espanola	Pacific	3	46.44	0.41	1.26	0.41	16.08	1.14	9.08	0.43	0.18	0.02	11.89	0.28	10.25	1.72	2.83	0.39	0.76	0.36	0.46	0.36
Fangatufa	Pacific	24	46.34	2.17	1.99	0.49	16.82	1.36	7.52	1.80	0.09	0.03	10.99	0.81	10.69	1.40	2.16	0.39	0.64	0.32	0.34	0.14

(continued on next page)

Table 2 (*continued*)

Island	Ocean	N	Si_{72}	Si_{72} σ	Ti_{72}	Ti_{72} σ	Al_{72}	Al_{72} σ	Fe_{72}	Fe_{72} σ	Mn_{72}	Mn_{72} σ	Mg_{72}	Mg_{72} σ	Ca_{72}	Ca_{72} σ	Na_{72}	Na_{72} σ	K_{72}	K_{72} σ	P_{72}	P_{72} σ
Fatu hiva	Pacific	29	45.16	2.11	3.02	0.58	15.60	2.75	9.12	1.91	0.14	0.04	12.26	1.66	9.86	1.39	2.21	0.32	1.05	0.46	0.42	0.13
Fatu huku	Pacific	15	46.61	0.81	2.70	0.17	12.18	2.80	10.23	1.71	0.15	0.03	13.38	1.91	8.86	0.82	2.24	0.27	1.34	0.34	0.48	0.11
Fernandina	Pacific	58	47.47	1.15	2.61	0.75	17.35	1.24	7.56	0.54	0.11	0.02	10.83	0.28	11.56	0.26	2.30	0.18	0.42	0.09	0.28	0.07
Floreana	Pacific	29	46.25	0.85	1.33	0.30	15.58	1.10	9.29	0.56	0.18	0.03	12.08	0.53	10.54	1.43	2.88	0.47	0.84	0.27	0.24	0.06
Gambier Islands	Pacific	15	48.11	0.76	1.85	0.25	16.31	1.47	8.19	0.97	0.11	0.03	11.33	0.82	10.67	0.91	1.98	0.17	0.49	0.16	0.33	0.08
Gardner Pinnacle	Pacific	2	44.76	2.04	1.38	0.12	17.59	2.32	7.19	0.09	0.09	0.09	10.77	0.04	11.17	1.81	2.38	0.39	1.56	1.62	0.15	0.20
Genovesa	Pacific	2	47.22	0.72	0.59	0.48	20.08	3.65	6.98	2.83	0.11	0.05	10.44	1.90	12.31	1.51	2.28	0.27	0.01	0.04	0.05	0.00
Hatutu	Pacific	20	45.45	3.15	2.33	0.57	13.15	2.44	9.87	1.78	0.14	0.04	12.84	1.84	11.47	2.33	2.10	0.17	0.84	0.20	0.43	0.07
Hawaii	Pacific	4682	49.02	3.70	1.87	0.44	15.27	2.11	9.04	1.87	0.14	0.38	12.02	1.42	10.59	2.23	2.12	0.60	0.48	0.38	0.28	0.20
Hiva oa	Pacific	40	46.45	2.40	2.73	0.81	16.38	3.19	7.73	3.25	0.12	0.05	11.65	1.99	9.00	1.55	2.60	0.53	1.66	0.59	0.49	0.15
Huahine	Pacific	7	46.91	0.70	2.57	0.12	11.82	1.12	10.62	0.80	0.14	0.01	13.87	0.96	8.04	0.45	2.25	0.19	1.61	0.30	0.42	0.05
Isabela	Pacific	224	48.49	1.20	2.05	0.34	17.43	1.25	8.03	0.96	0.12	0.02	11.20	0.75	11.08	0.98	2.66	0.28	0.52	0.13	0.32	0.10
Isla Isabela	Pacific	30	47.52	0.75	1.77	0.22	16.17	1.02	8.93	0.46	0.14	0.01	11.69	0.35	12.03	0.83	2.32	0.22	0.43	0.06	0.22	0.04
Kahoolawe	Pacific	65	49.92	2.19	1.76	0.27	16.12	1.72	8.68	1.58	0.12	0.05	11.71	1.39	9.72	1.37	2.29	0.48	0.43	0.46	0.31	0.18
Kauai	Pacific	191	42.61	5.16	2.24	0.53	12.59	2.14	11.92	1.69	0.16	0.03	14.90	1.72	10.97	3.40	2.15	0.74	0.60	0.37	0.45	0.23
La Perouse Pinnacle	Pacific	6	40.14	9.29	1.96	0.07	12.00	2.51	12.03	0.43	0.17	0.02	14.62	1.67	14.85	7.37	2.09	0.72	0.43	0.11	0.60	0.33
Lanai	Pacific	23	50.25	1.34	1.56	0.19	14.84	1.77	9.31	1.22	0.13	0.03	12.27	1.27	8.94	0.87	1.60	0.35	0.18	0.15	0.14	0.06
Macquarie Island	Pacific	57	48.50	0.78	1.28	0.16	17.66	0.66	6.98	0.56	0.10	0.03	10.08	0.51	10.35	0.84	3.01	0.42	0.70	0.35	0.28	0.12
Mangaia	Pacific	55	43.15	1.38	2.05	0.59	15.04	3.47	9.92	2.50	0.14	0.04	12.75	2.00	12.26	1.49	2.40	0.60	0.77	0.29	0.38	0.12
Marchena	Pacific	11	47.89	10.23	1.39	0.43	17.61	3.96	8.58	2.27	0.13	0.04	11.50	2.68	12.24	2.86	2.79	0.65	0.25	0.13	0.17	0.07
Mas a Tierra	Pacific	38	44.00	3.19	2.40	0.68	14.02	2.54	10.64	2.25	0.15	0.05	13.91	2.31	9.85	2.27	2.98	0.72	0.99	0.49	0.51	0.15
Mas Afuera	Pacific	11	44.55	7.26	2.07	0.31	14.95	2.84	10.91	3.02	0.13	0.06	14.19	3.23	9.76	4.56	2.55	0.30	0.64	0.17	0.39	0.15
Matotiri	Pacific	6	43.36	1.63	1.88	0.88	18.00	6.02	6.67	3.84	0.10	0.05	11.56	2.49	11.67	0.42	3.23	1.05	1.37	0.47	0.78	0.22
Maui	Pacific	271	45.89	3.05	2.07	0.61	16.57	2.85	8.82	2.65	0.13	0.03	12.10	1.77	10.60	1.36	2.71	1.01	0.82	0.56	0.39	0.17
Mehetia	Pacific	45	44.10	1.38	3.10	0.45	13.80	2.96	10.21	2.30	0.13	0.03	13.31	2.12	9.60	0.92	2.74	0.37	1.68	0.56	0.58	0.13
Molokai	Pacific	145	46.84	2.07	2.02	0.45	16.50	2.50	8.74	2.24	0.12	0.03	12.02	1.67	10.48	1.19	2.37	0.55	0.59	0.35	0.39	0.23
Motane	Pacific	6	46.19	1.55	2.85	0.58	17.96	2.54	7.17	2.44	0.13	0.04	11.02	1.47	9.14	0.67	2.55	0.41	1.19	0.33	0.49	0.10
Motu nao	Pacific	5	47.21	2.47	2.15	1.25	17.50	3.80	6.64	3.52	0.15	0.08	11.10	1.77	10.15	1.71	3.12	0.69	2.02	0.66	0.60	0.26
Mururoa atoll	Pacific	43	43.55	2.47	2.35	0.80	17.11	2.92	7.60	2.76	0.09	0.04	11.42	2.04	6.19	4.45	1.77	0.76	4.62	3.94	0.89	0.50
Nihoa	Pacific	6	47.83	2.36	2.33	0.40	14.63	2.40	9.80	1.83	0.11	0.03	12.77	2.14	9.11	0.96	2.08	0.32	0.33	0.20	0.49	0.37
Niihau	Pacific	8	45.57	2.11	1.69	0.52	15.98	0.94	9.66	1.01	0.13	0.05	12.54	1.04	10.42	0.86	2.38	0.33	0.47	0.17	0.26	0.16
Nuku hiva	Pacific	81	46.42	1.66	2.24	0.56	17.22	2.16	7.30	2.20	0.11	0.04	11.15	1.25	9.14	1.26	2.63	0.58	1.58	0.48	0.47	0.14
Oahu	Pacific	492	47.58	5.25	1.80	0.37	14.54	3.11	9.34	1.81	0.13	0.07	12.25	1.53	9.62	1.74	2.49	0.84	0.49	0.39	0.36	0.29
Pinta	Pacific	20	48.28	0.96	1.64	0.63	19.02	3.89	6.81	2.06	0.10	0.04	10.26	1.38	11.59	1.06	2.51	0.35	0.53	0.21	0.28	0.11
Pinzon	Pacific	13	47.80	1.10	1.61	0.45	17.95	1.69	7.80	1.35	0.12	0.02	11.04	0.65	11.16	0.71	2.51	0.24	0.41	0.20	0.27	0.08
Pitcairn	Pacific	19	47.82	1.33	2.08	0.73	19.40	1.45	6.17	1.53	0.09	0.03	10.58	0.50	9.54	0.59	3.28	0.41	1.53	0.31	0.54	0.19
Rabida	Pacific	5	48.68	0.42	1.79	0.64	18.19	0.33	6.85	0.11	0.10	0.03	10.58	0.57	10.58	0.52	3.10	0.44	0.56	0.23	0.36	0.15
Raiatea	Pacific	4	41.06	4.34	2.59	1.30	12.96	3.09	11.46	2.88	0.15	0.04	14.67	3.03	11.80	3.25	2.22	0.37	0.99	0.43	0.53	0.07
Raivavae	Pacific	29	45.43	2.84	1.71	0.51	14.83	3.59	9.41	2.49	0.13	0.04	12.87	2.21	10.90	2.12	2.46	0.53	0.65	0.18	0.35	0.14
Rapa	Pacific	21	42.26	6.81	2.78	0.79	14.44	3.57	10.11	2.93	0.13	0.04	13.46	2.18	11.47	5.75	2.38	0.77	1.18	0.48	0.62	0.20
Rarotonga	Pacific	11	44.11	2.33	2.58	0.76	14.48	4.51	8.92	3.45	0.16	0.03	12.75	2.62	11.00	1.53	2.37	0.89	1.75	1.03	0.68	0.34
Rimatara	Pacific	3	43.18	1.76	2.31	0.83	15.33	2.98	9.32	1.99	0.13	0.03	12.31	1.71	10.62	2.57	2.57	1.30	1.83	0.48	0.68	0.42
Roca Redonda	Pacific	23	45.88	2.08	2.13	0.39	14.33	3.09	10.79	2.55	0.15	0.05	14.26	2.67	9.34	1.32	2.95	0.39	0.64	0.10	0.41	0.07
Ross Island	Pacific	18	45.92	3.05	1.64	1.10	19.55	3.44	5.38	3.45	0.14	0.03	10.58	1.67	9.02	2.25	4.59	0.84	2.19	0.67	1.02	0.34
Rututu	Pacific	41	43.70	1.53	2.23	0.49	15.34	3.06	9.67	2.05	0.13	0.03	12.52	1.80	11.22	1.62	2.47	1.00	0.67	0.46	0.52	0.35
San Cristobal	Pacific	5	46.64	1.09	1.37	0.42	17.32	1.99	8.75	0.54	0.18	0.04	11.60	0.50	10.60	1.09	2.55	0.34	0.51	0.22	0.20	0.06
Santa Cruz	Pacific	9	46.30	1.16	1.50	0.23	16.84	1.09	9.88	0.39	0.15	0.03	12.66	0.56	9.15	0.98	2.66	0.41	0.22	0.10	0.20	0.09
Santa Fe	Pacific	10	47.60	1.55	1.58	0.44	17.77	0.78	8.30	1.18	0.17	0.06	11.38	0.79	9.63	0.83	3.06	0.34	0.56	0.23	0.38	0.17
Savaii	Pacific	31	45.97	1.01	2.91	0.39	13.51	1.65	10.69	0.84	0.14	0.02	13.73	1.03	8.39	0.82	2.80	0.46	1.42	0.44	0.41	0.12
Tahaa	Pacific	12	46.79	1.52	2.69	0.33	12.99	2.26	9.84	1.29	0.14	0.07	12.91	1.07	8.49	1.70	1.94	0.71	1.48	0.48	0.42	0.13
Tahiti	Pacific	111	44.33	2.42	2.58	0.67	14.58	3.94	9.24	3.12	0.12	0.05	12.72	2.34	11.10	2.92	2.54	0.95	1.34	0.66	0.58	0.33
Tahuata	Pacific	18	45.08	2.36	2.74	0.64	15.64	3.55	8.76	2.68	0.11	0.06	12.15	2.08	10.30	1.68	2.54	0.82	1.36	0.68	0.36	0.21
Tubuai	Pacific	105	41.83	2.27	2.01	0.53	15.16	2.84	10.09	2.13	0.18	0.04	12.76	1.68	11.63	2.11	3.20	1.41	0.98	0.40	0.60	0.28
Tutuila	Pacific	23	45.59	2.04	3.03	0.73	14.61	3.10	9.85	2.31	0.12	0.04	13.02	1.89	9.20	0.77	2.58	0.47	1.20	0.33	0.49	0.14
Ua Huka	Pacific	12	44.61	2.10	2.70	0.43	15.22	3.10	9.03	2.17	0.13	0.03	12.32	1.73	9.85	1.15	2.48	0.66	1.24	0.57	0.42	0.06
Ua pou	Pacific	50	44.34	2.48	2.52	0.77	17.28	2.62	7.66	3.09	0.14	0.10	11.32	1.64	9.90	1.28	3.02	0.85	1.54	1.07	0.65	0.22
Upolu	Pacific	54	44.97	2.68	3.31	0.86	14.91	2.51	9.98	2.31	0.12	0.03	12.85	1.80	9.95	0.96	2.62	0.63	1.17	0.43	0.51	0.16
Wolf	Pacific	2	48.26	0.80	0.53	0.12	20.64	4.89	6.03	3.01	0.08	0.05	9.74	1.93	12.68	0.96	2.30	0.32	0.16	0.05	0.41	0.04

Data source: http://georoc.mpch-mainz.gwdg.de/georoc/Entry.html.
N refers to the number of samples available for averaging; σ refers to one standard deviation from the mean.

Table 3
Average La/Sm and Sm/Yb ratios of ocean island basalts normalized to chondrite.

Island	Ocean	$[La/Sm]_{CN}$			$[Sm/Yb]_{CN}$		
		N	*Mean*	*σ*	*N*	*Mean*	*σ*
Ascension	Atlantic	30	2.770	0.517	27	2.748	0.727
Bioko	Atlantic	3	3.267	0.508	N/A	N/A	N/A
Boa Vista	Atlantic	N/A	N/A	N/A	N/A	N/A	N/A
Chao	Atlantic	19	2.985	0.652	19	4.246	0.574
Deserta grande	Atlantic	44	2.599	0.369	44	3.868	0.704
Faial	Atlantic	31	3.394	0.648	30	3.461	0.596
Fernando poo	Atlantic	N/A	N/A	N/A	N/A	N/A	N/A
Flores	Atlantic	5	4.134	0.870	5	4.271	0.265
Fogo	Atlantic	19	3.125	0.406	19	6.033	0.494
Fuerteventura	Atlantic	24	3.022	0.469	24	6.153	1.325
Gough	Atlantic	12	4.676	1.655	11	4.940	1.286
Graciosa	Atlantic	5	3.136	0.715	5	3.817	0.660
Gran Canaria	Atlantic	86	3.455	1.207	73	5.864	2.386
Hierro	Atlantic	3	2.544	0.391	3	6.400	0.876
Iceland	Atlantic	823	1.468	0.879	792	1.724	0.697
Inaccessible	Atlantic	7	3.835	0.179	7	5.032	0.266
Jan Mayen	Atlantic	24	4.346	1.201	23	4.062	0.491
Kolbeinsey	Atlantic	2	0.422	0.190	2	0.671	0.080
La Gomera	Atlantic	11	6.788	3.676	10	4.880	6.450
La Palma	Atlantic	24	5.071	1.536	15	5.634	0.220
Lanzarote	Atlantic	42	3.277	1.256	42	5.044	1.019
Maderia	Atlantic	72	3.450	0.737	66	4.650	0.545
Maio	Atlantic	11	1.511	1.398	11	3.149	2.997
Pagalu	Atlantic	25	3.836	2.787	10	5.141	1.883
Pico	Atlantic	15	2.894	0.400	15	3.366	0.387
Porto Santo	Atlantic	14	4.155	1.356	14	3.917	0.904
Principe	Atlantic	8	7.292	9.995	N/A	N/A	N/A
Sal	Atlantic	3	3.403	0.562	3	6.734	0.090
Santiago	Atlantic	11	3.691	0.299	11	6.516	1.048
Sao Jorge	Atlantic	10	2.689	0.192	10	4.287	0.766
Sao Miguel	Atlantic	28	3.913	0.986	36	4.350	0.719
Sao Tome	Atlantic	3	4.503	0.470	N/A	N/A	N/A
St Helena	Atlantic	50	3.919	1.696	48	4.126	1.056
Tenerife	Atlantic	164	5.370	3.482	168	4.477	1.673
Terceira	Atlantic	13	3.417	2.604	16	3.365	1.118
Trinidade	Atlantic	46	6.808	2.732	33	5.002	2.063
Tristan da cuhna	Atlantic	13	5.144	3.787	10	5.270	1.109
Vestmannaeyjar islands	Atlantic	35	1.717	0.224	37	2.207	0.142
Amsterdam	Indian	N/A	N/A	N/A	N/A	N/A	N/A
Foch	Indian	29	2.151	0.327	29	3.044	0.505
Heard	Indian	16	3.217	0.714	14	6.093	1.565
Ile aux Cochon	Indian	N/A	N/A	N/A	N/A	N/A	N/A
Ile de la Possession	Indian	N/A	N/A	N/A	N/A	N/A	N/A
Ile de L'est	Indian	N/A	N/A	N/A	N/A	N/A	N/A
Ile de L'ouest	Indian	176	3.055	1.724	176	3.640	1.153
Kerguelen	Indian	4	4.210	0.349	3	4.713	2.002
Mauritius	Indian	16	2.004	0.481	16	2.814	0.873
Reunion	Indian	163	2.158	0.194	201	3.256	0.314
Aitutaki	Pacific	9	4.022	0.667	8	6.771	1.979
Atiu	Pacific	8	3.188	0.506	7	4.874	0.849
Baltra	Pacific	N/A	N/A	N/A	N/A	N/A	N/A
Bora Bora	Pacific	10	2.479	0.457	9	4.351	0.813
Darwin	Pacific	4	1.441	0.060	4	2.174	0.798
Easter Island	Pacific	41	2.102	0.520	38	2.333	0.368
Eiao	Pacific	36	1.764	0.451	36	4.190	0.552
Espanola	Pacific	2	2.123	0.107	3	1.680	0.175
Fangatufa	Pacific	14	2.309	0.279	13	4.490	0.572
Fatu hiva	Pacific	4	2.914	0.158	4	5.148	0.698
Fatu huku	Pacific	4	2.121	0.245	4	4.325	0.181
Fernandina	Pacific	35	1.676	0.050	35	2.644	0.160
Floreana	Pacific	20	3.662	1.602	19	1.782	0.218
Gambier Islands	Pacific	9	2.205	0.148	9	3.582	0.247
Gardner Pinnacle	Pacific	N/A	N/A	N/A	N/A	N/A	N/A
Genovesa	Pacific	5	0.491	0.020	6	1.163	0.034
Hatutu	Pacific	5	2.135	0.333	5	4.179	0.459
Hawaii	Pacific	837	1.561	0.631	877	3.085	0.640
Hiva oa	Pacific	12	2.425	0.272	12	4.381	1.044
Huahine	Pacific	10	3.180	0.572	9	5.050	0.452
Isabela	Pacific	121	1.921	0.712	121	2.658	0.666
Isla Isabela	Pacific	13	2.091	0.197	13	2.527	0.253
Kahoolawe	Pacific	66	1.612	0.328	59	2.849	0.541
Kauai	Pacific	71	2.442	0.527	71	5.596	1.578
La Perouse Pinnacle	Pacific	N/A	N/A	N/A	N/A	N/A	N/A

(continued on next page)

Table 3 (*continued*)

Island	Ocean	[La/Sm]$_{CN}$			[Sm/Yb]$_{CN}$		
		N	*Mean*	σ	*N*	*Mean*	σ
Lanai	Pacific	25	1.211	0.139	25	2.591	0.331
Macquarie Island	Pacific	58	3.114	0.916	58	1.868	0.393
Mangaia	Pacific	40	3.058	0.395	40	4.369	0.245
Marchena	Pacific	11	0.971	0.056	11	1.609	0.110
Mas a Tierra	Pacific	6	3.049	0.856	6	3.822	0.420
Mas Afuera	Pacific	1	1.937	N/A	1	3.111	N/A
Matotiri	Pacific	4	3.030	0.290	4	5.050	0.234
Maui	Pacific	187	2.001	0.699	184	3.741	0.801
Mehetia	Pacific	13	2.562	0.123	15	6.673	0.431
Molokai	Pacific	57	2.843	2.718	55	4.099	1.836
Motane	Pacific	N/A	N/A	N/A	N/A	N/A	N/A
Motu nao	Pacific	3	3.316	0.450	3	5.171	0.315
Mururoa atoll	Pacific	49	2.741	0.664	49	5.810	0.961
Nihoa	Pacific	N/A	N/A	N/A	N/A	N/A	N/A
Niihau	Pacific	N/A	N/A	N/A	N/A	N/A	N/A
Nuku hiva	Pacific	54	4.085	1.987	54	4.107	0.930
Oahu	Pacific	255	1.671	0.765	248	3.861	2.264
Pinta	Pacific	9	2.002	0.190	8	2.578	0.289
Pinzon	Pacific	22	1.760	0.322	21	2.224	0.174
Pitcairn	Pacific	4	3.225	0.353	4	4.699	0.818
Rabida	Pacific	9	2.354	0.936	6	2.746	0.308
Raiatea	Pacific	2	2.524	0.019	2	7.384	0.427
Raivavae	Pacific	29	3.330	1.157	29	4.363	0.811
Rapa	Pacific	17	2.817	0.260	16	6.703	1.658
Rarotonga	Pacific	11	6.657	3.740	10	4.808	1.599
Rimatara	Pacific	3	2.913	0.535	3	5.266	1.137
Roca Redonda	Pacific	3	1.945	0.013	3	2.944	0.038
Ross Island	Pacific	49	5.049	1.847	49	3.915	0.860
Rututu	Pacific	30	2.911	0.485	29	4.563	0.878
San Cristobal	Pacific	9	1.606	0.563	9	1.448	0.406
Santa Cruz	Pacific	20	1.234	0.243	19	1.749	0.277
Santa Fe	Pacific	3	1.464	0.635	3	1.979	0.651
Savaii	Pacific	31	2.929	0.441	29	4.945	0.932
Tahaa	Pacific	34	2.728	1.506	33	3.965	1.979
Tahiti	Pacific	90	3.199	3.893	50	5.257	1.222
Tahuata	Pacific	10	2.216	1.143	10	5.084	1.217
Tubuai	Pacific	31	4.301	1.145	26	5.204	1.041
Tutuila	Pacific	4	1.735	0.402	4	4.509	1.313
Ua Huka	Pacific	N/A	N/A	N/A	N/A	N/A	N/A
Ua pou	Pacific	18	3.469	1.459	18	4.934	0.836
Upolu	Pacific	32	2.829	0.586	31	5.312	1.130
Wolf	Pacific	2	1.448	0.004	2	1.617	0.059

Data source: http://georoc.mpch-mainz.gwdg.de/georoc/Entry.html.
N refers to the number of samples available for averaging; σ refers to one standard deviation from the mean.
Data normalised to chondrite; Sun and McDonough (1989).

thickness for older lithosphere. In some cases, a relative age of the lithosphere had previously been determined in other studies (e.g., Haase, 1996). This provides a useful constraint on our calculation. The two datasets were compared and a good agreement was found between the datasets.

4. Results

4.1. Fractionation corrected major element variation as a function of lithosphere thickness

Table 2 gives the averages of major element compositions corrected from fractionation effect to $Mg^{\#}=0.72$ following Niu et al. (1999) and Niu and O'Hara (2008) (also see above and Appendix A) for all the 115 volcanic islands. These fractionation-corrected compositions do not represent primary mantle melts, but melts of Moho-crossing compositions and record signatures of mantle (vs. crustal) processes. These include fertile mantle compositional variation, the extent and depth range of melting and melt–solid interaction during ascent in the mantle. As a result, large compositional scatter from a given volcanic island (i.e., 1σ variation in Table 2), between volcanic islands, and between island groups from geographically different regions and ocean basins is therefore expected. This is true particularly for highly incompatible elements like K_2O. However, the statistically significant correlation of island-averaged OIB compositions (individual data points) with lithosphere thickness is remarkable (Fig. 3). The LLDs used to correct for fractionation effect, whether based on MORB or OIB, do not affect the first-order trend of OIB chemistry with lithosphere thickness, which in turn reflects mantle (vs. crustal) processes. Hence, the subsequent discussion focuses on MORB LLD-corrected data and plots in left columns of Fig. 3 only for clarity and convenience.

Fig. 3 shows that despite the scatter for reasons discussed above, Si_{72} and Al_{72} decrease whereas Fe_{72} and Mg_{72} increase with increasing lithosphere thickness, which is consistent with increasing pressures of melting (e.g., Niu and Batiza, 1991; Niu, 1997; Walter, 1998; also see below) from beneath thin lithosphere to beneath thick lithosphere. The weak Ca_{72} decrease with increasing lithosphere thickness is also consistent with the weak negative CaO-pressure dependence (Niu, 1997; Walter, 1998). On the other hand, the systematic increase in Ti_{72} and P_{72} with increasing lithosphere thickness is consistent with decreasing extent of melting (Niu, 1997; Walter, 1998) from beneath thin lithosphere to beneath thick lithosphere because these two elements are incompatible during mantle melting. While Na_2O is often treated as an incompatible element during mantle melting, it becomes less incompatible with increasing melting pressure (Blundy et al., 1995), which explains why Na_{72} does not show a systematic increase with increasing lithosphere thickness (less incompatible with increasing melting pressure). All these are qualitatively consistent with the conceptual expectations illustrated in Fig. 1.

4.2. $[La/Sm]_{CN}$ and $[Sm/Yb]_{CN}$ variation as a function of lithosphere thickness

Table 3 gives the averages of chondrite-normalized La/Sm and Sm/Yb ratios for the 115 volcanic islands where data are available. Fig. 4 shows, despite the large variation defined by samples within and between individual volcanic islands, island-averaged $[La/Sm]_{CN}$ and $[Sm/Yb]_{CN}$ ratios show significant positive correlations with lithosphere thickness. This is also consistent with decreasing extent of melting from beneath thin lithosphere to beneath thick lithosphere because La is more incompatible than Sm, and Sm is more incompatible than Yb during mantle melting. Note that the greater than unity $[Sm/Yb]_{CN}$ values for all but one volcanic island indicate the presence of the familiar "garnet signature" in these OIB melts as expected. However, it should be noted that the intensity of the garnet signature increases in OIB melts with increasing lithosphere thickness. This is again consistent with increasing pressure of melting and decreasing extent of melting from beneath thin lithosphere to beneath thick lithosphere in agreement with inferences from major elements (Fig. 3). The term "garnet signature" has been used to describe geochemical signals in the melt reflecting that garnet is a residual phase during mantle melting (Salters and Hart, 1989; Hirschmann and Stolper, 1996; Niu et al., 1999). The basic concept is based on the understanding that among all the major silicate minerals in mantle source regions for basalts, garnet is unique in having over 2 orders of magnitude variation in its partition coefficients so that while light REEs are incompatible in garnet, heavy REEs are strongly compatible in garnet (Irving and Frey, 1978). Consequently, high $[Sm/Yb]_{CN}$ ratios in basalts would suggest the presence of garnet as a residual phase in the source region that preferentially holds heavy REEs (e.g., Yb vs. Sm, which is an intermediate REE).

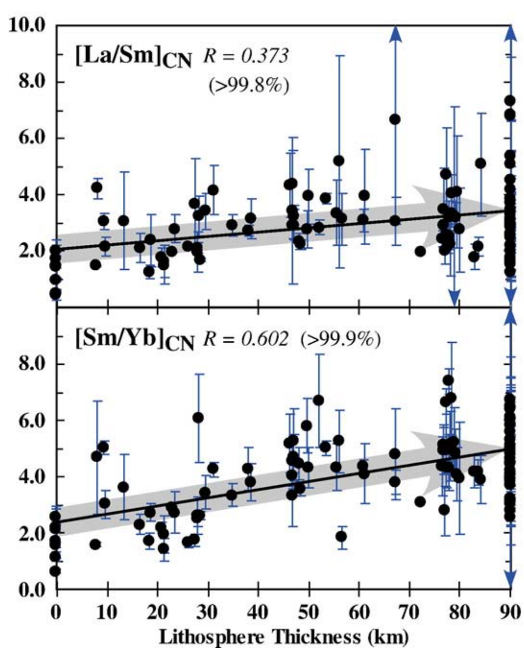

Fig. 4. Island-averaged La/Sm and Sm/Yb ratios normalized to C1 chondrite values (Sun and McDonough, 1989) plotted against oceanic lithosphere thickness (see Table 3). The systematic increase in $[La/Sm]_{CN}$ and $[SM/Yb]_{CN}$ with increasing lithosphere thickness is also consistent with increasing pressure and decreasing extent of melting from beneath thin lithosphere to beneath thick lithosphere (see text for details).

4.3. Binary co-variations

Fig. 5 shows co-variations of major elements corrected for fractionation effect to $Mg^{\#} = 0.72$ and $[La/Sm]_{CN}$ and $[Sm/Yb]_{CN}$ ratios using island-averaged data points (Tables 2 and 3). Given the fact that each data point represents a volcanic island, these statistically significant correlations are indicative of a common process influencing OIB petrogenesis on a global scale. Indeed, the data trends (arrowed thick regression lines) are consistent with increasing pressure and decreasing extent of melting from beneath thin lithosphere to beneath thick lithosphere. It is important to note that the binary co-variations of these petrological parameters (Fig. 5; Table 4) are in general more significant than their correlations with lithosphere thickness (Figs. 3 and 4). The better correlations in Fig. 5 are partly caused by the data closure for major (and minor) elements because their sum for each sample or each island average is constrained to ~100%. On the other hand, the more significant binary correlations involving ratios (i.e., $[La/Sm]_{CN}$ and $[La/Sm]_{CN}$) do not result from the data closure, but a genuine effect. If we neglected the effect of lithosphere thickness variation in our interpretation on the basis of Figs. 3 and 4, then the significant correlations in Fig. 5 state that island-averaged OIB data exhibit a straightforward inverse correlation between the extent and pressure of melting on a global scale. This means that some of the scattered data points in Figs. 3 and 4 have become part of the main trend in Fig. 5, leading to improved correlations (see below). Finally, knowing that Na_{72} shows no correlation with lithosphere thickness (Fig. 3), the positive Na_{72}-$[La/Sm]_{CN}$ correlation suggests source compositional variation beyond the effect of the extent and pressure of melting as a function of lithosphere thickness variation.

5. Discussion

5.1. Oceanic lithosphere thickness control on OIB compositions

Peridotite melting experiments under both spinel peridotite (e.g., Jaques and Green, 1980) and garnet peridotite (e.g., Walter, 1998) facies conditions have consistently shown that FeO and MgO increase whereas SiO_2 and Al_2O_3 decrease in the partial melt with increasing pressure as has been successfully modelled (Niu and Batiza, 1991; Niu, 1997; Walter, 1998). Incompatible elements such as TiO_2 and P_2O_5 in the partial melt decrease with increasing extent of melting. It follows from Figs. 3 and 4 that island-averaged compositions of OIB are consistent with increasing pressure and decreasing extent of melting from beneath thin lithosphere to beneath thick lithosphere. Furthermore, all but one island-averaged $[Sm/Yb]_{CN}>1$ (Fig. 4), which indicates that mantle melting for OIB begins in the garnet peridotite facies, and the intensity of the garnet signature increases progressively in the melt produced beneath the thickened lithosphere.

These observations can be readily explained in terms of the familiar concept illustrated in Fig. 6 (modified from Niu and Hékinian, 1997; Niu et al., 2001; Niu and O'Hara, 2008). Assuming melting in the sub-lithospheric mantle results from decompression of an adiabatically upwelling parcel of mantle, the mantle will begin to melt when it intersects the solidus. Continued upwelling is accompanied by continued decompression melting. As a result, the amount of melt produced or the extent of melting from a given parcel of mantle is proportional to the amount of vertical decompression. The lithosphere thus limits the vertical extent of decompression. Melting beneath thick lithosphere stops at a greater depth, produces less melt (high Ti and P) with a high pressure signature (high Fe_{72}, Mg_{72} and low Si_{72} and Al_{72}) whereas melting beneath thin lithosphere stops at a shallow depth, produces more melt (low Ti and P) with a low pressure signature (low Fe_{72}, Mg_{72} and high Si_{72} and Al_{72}). It follows that the intensity of the garnet signature in OIB depends on the relative proportion of melt that is produced in the garnet (vs. spinel) peridotite facies. With decreasing

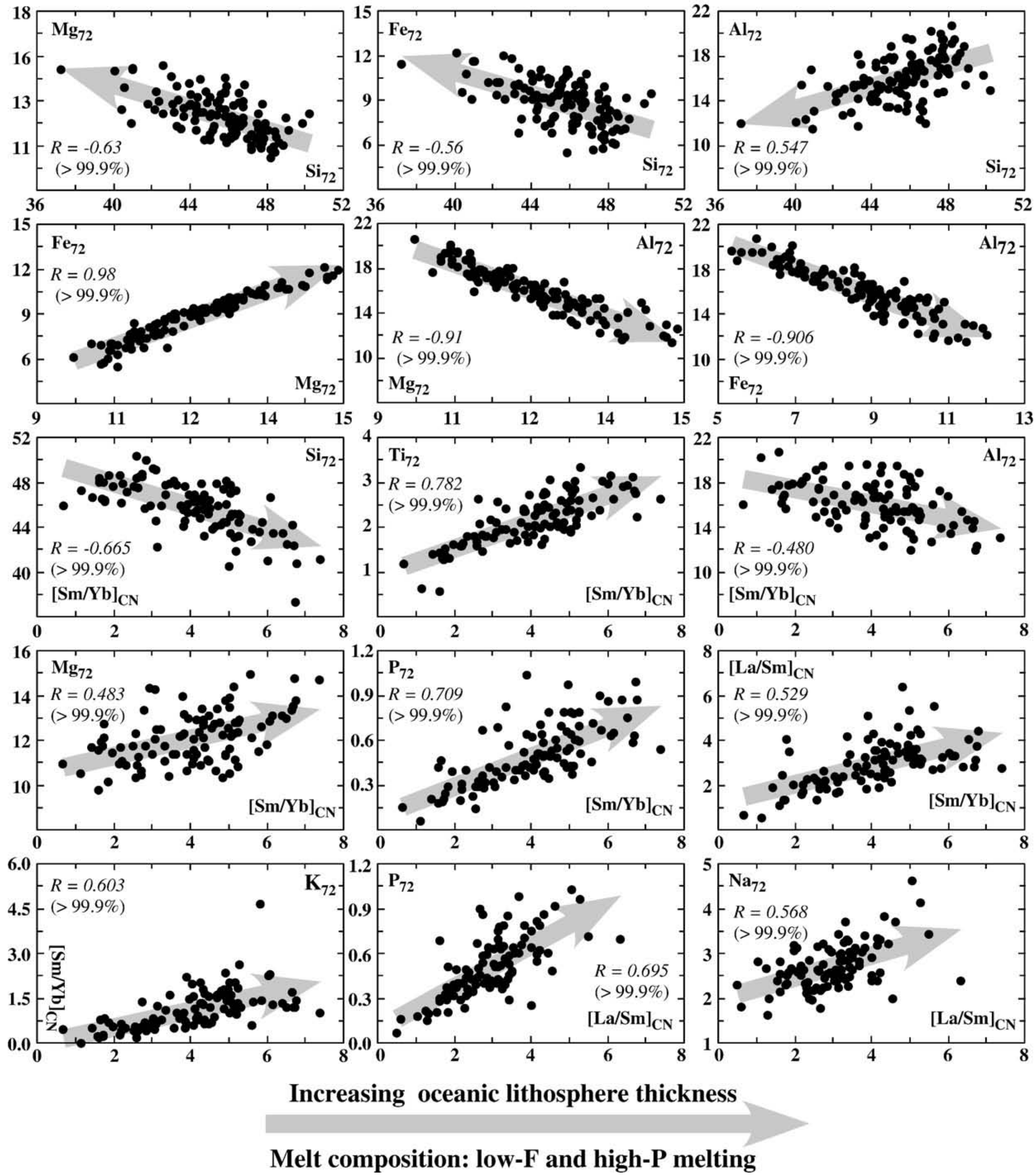

Fig. 5. Co-variation diagrams showing statistically significant correlations among all the island-averaged petrologic and geochemical parameters (see Tables 2–4) with the trend indicated by the thick and arrowed regression lines pointing to decreasing extent and increasing pressure of melting, which is consistent with the lithosphere thickness control, i.e., from beneath thin lithosphere to beneath thick lithosphere. Note the improved (vs. Figs. 3 and 4) correlations result from the fact that some of the scattered data points in Figs. 3 and 4 become part of the main trends here, mostly caused by fertile mantle compositional control. The remaining scatter is likely a combined effect of "OIB source" compositional variation and uncertainties associated the analytical data and correction procedures.

lithosphere thickness, the extent of melting increases with more melt produced by decompression in the spinel peridotite facies. As a result, the intensity of the garnet signature in OIB melts is inversely related to the extent of dilution; it is diluted less in melts produced by low extents of melting beneath thick lithosphere and is diluted more in melts produced by high extents of melting beneath thin lithosphere (Niu et al., 1999; Niu and O'Hara, 2008).

It is important to note that for conceptual clarity, we assumed a constant mantle solidus depth beneath all islands in Fig. 6. Strictly speaking, this assumption is unjustified as the solidus is a material property and its depth depends on fertile mantle composition, in particular the alkali and volatile contents (Wyllie, 1971; Green, 1973), which determines the initial depth of melting and thus affects the extent of melting, yet we do have any direct information on the mantle solidus depth beneath individual ocean islands. Furthermore, mantle potential temperature also affects the depth of the solidus, and thus the extent of decompression melting and OIB compositions. However, the mantle potential temperature cannot be constrained with the existing data. Nevertheless, the significant OIB compositional correlations with the thickness of the oceanic lithosphere (Figs. 3 and 4) attest that the lithosphere thickness exerts the first-order control on the geochemistry of OIB on a global scale.

Table 4
Correlation coefficients between petrologic parameters.

	Lithosphere thickness (km)	Si_{72}	Ti_{72}	Al_{72}	Fe_{72}	Mn_{72}	Mg_{72}	Ca_{72}	Na_{72}	K_{72}	P_{72}	$[La/Sm]_{CN}$	$[Sm/Yb]_{CN}$
Lithosphere thickness (km)	1.000												
Si_{72}	− 0.439	1.000											
Ti_{72}	0.567	−0.539	1.000										
Al_{72}	−0.500	0.547	−0.611	1.000									
Fe_{72}	*0.389*	−0.568	0.477	−0.906	1.000								
Mn_{72}	0.170	−0.439	0.156	−0.541	0.594	1.000							
Mg_{72}	0.457	−0.630	0.545	−0.912	0.958	0.572	1.000						
Ca_{72}	−0.120	*−0.358*	−0.184	−0.051	0.131	0.206	0.065	1.000					
Na_{72}	0.076	−0.156	0.063	*0.321*	*−0.357*	0.038	−0.250	−0.144	1.000				
K_{72}	0.268	−0.262	*0.397*	0.009	−0.189	−0.149	−0.052	−0.440	*0.358*	1.000			
P_{72}	0.425	−0.597	0.515	−0.160	0.031	0.158	0.188	−0.088	0.574	0.673	1.000		
$[La/Sm]_{CN}$	*0.373*	*−0.356*	*0.320*	−0.007	−0.126	0.088	0.004	−0.165	0.568	0.575	0.695	1.000	
$[Sm/Yb]_{CN}$	0.606	−0.665	0.782	−0.480	*0.334*	0.012	0.483	−0.117	0.189	0.603	0.709	0.529	1.000

For N = 115 (major elements), N = 102 (La/Sm) and N = 99 (Sm/Yb), data set in bold are statistically significant; non-italics are significant at >99.9% (R>0.400 or R<**−0.400**) confidence level; italics are significant at >99.8% confidence level (R>0.321 or R–*0.321*).

5.2. Fertile mantle compositional control on OIB compositions

Fertile mantle source heterogeneity is required to explain the large OIB compositional variation on a given island, between islands and between island groups (Figs. 3 and 4). The OIB source heterogeneity is likely to have multiple origins such as recycled oceanic crust (e.g., Hofmann and White, 1982; Niu and Batiza, 1997), recycled terrigeneous sediments (e.g., Chauvel et al., 1992; White and Duncan, 1996; Hofmann, 1997) and mantle metasomatism (e.g., Green, 1971; Frey and Green, 1974; Sun and Hanson, 1975; Lloyd and Bailey, 1975; Frey and Green, 1978; Wood, 1979; Menzies and Hawkesworth, 1987; Le Roex et al., 1983; O'Reilly and Griffin, 1988; Sun and McDonough, 1989; Anderson, 1994; McKenzie and O'Nions, 1995; Halliday et al., 1995; Niu et al., 1996, 1999, 2002; Niu and O'Hara, 2003; Donnelly et al., 2004; Workman et al., 2004; Pilet et al., 2005, 2008; Niu, 2008).

Recycled oceanic crust as a solidified mantle melt in composition should have elevated abundances of incompatible elements. However, the ocean crust is depleted in the progressively more incompatible elements (e.g., $[La/Sm]_{PM\ (Ocean\ Crust)}<1$; Niu, 2004) (subscript "PM" refers to normalized ratio against the primitive mantle), and thus cannot readily explain the incompatible element enriched nature of OIB ($[La/Sm]_{PM\ (OIB)}>>1$; Niu and O'Hara, 2003). Recycled terrigeneous sediments (i.e., upper continental crustal material) with $[La/Sm]_{PM\ (sediments)}\approx[La/Sm]_{PM\ (OIB)}>>1$) could be potentially important for OIB. However, primitive mantle normalized Nb/Th and Ta/U ratios are significantly less than unity, i.e., $[Nb/Th]_{PM}<<1$ and $[Ta/U]_{PM}<<1$ in the bulk continental crust (0.17 and 0.28 respectively; Rudnick and Gao, 2003) and in average sediments (0.15 and 0.19 respectively; Plank and Langmuir, 1998), but $[Nb/Th]_{PM}>1$ and $[Ta/U]_{PM}>1$ in oceanic basalts (including OIB) (Niu et al., 1999; Niu and O'Hara, 2009-this issue). Therefore, it remains unclear how recycled terrigeneous sediments may actually contribute to the OIB petrogenesis.

The recognition that OIB source materials are more enriched in incompatible elements than the primitive mantle (e.g., Sun and McDonough, 1989; McKenzie and O'Nions, 1995; Niu et al., 2002; Niu and O'Hara, 2003; Prytulak and Elliott, 2007) and are more enriched in the progressively more incompatible elements (e.g., $[La/Sm]_{OIB\ Source}>[La/Sm]_{PM}$; Sun and McDonough, 1989; Niu and O'Hara, 2003) suggests that the OIB source materials have undergone a low-degree melt enrichment process or mantle metasomatism. The mantle metasomatism has been described as mantle peridotites (whether primitive mantle or previously depleted melting residues) being infiltrated by a "low-degree melt" (low-F melt) that is enriched in volatiles (e.g., H_2O and CO_2) and incompatible elements inferred from studies of mantle melts (e.g., Sun and Hanson, 1975; Lloyd and Bailey, 1975; Sun and McDonough, 1989) and metasomatic minerals (e.g., amphibole, phlogopite) and vein lithologies (e.g., garnet pyroxenite, pyroxenite and hornblendite) from mantle xenoliths (e.g., Frey and Green, 1974, 1978; Menzies and Hawkesworth, 1987; O'Reilly and Griffin, 1988) and massif peridotites on land (Frey et al., 1985; Takazawa et al., 2000; Pilet et al., 2005) and mantle xenoliths from ocean islands (e.g., Frey, 1980; Sen et al., 2005).

However, discussions on where such low-F melt metasomatism may take place in the mantle are few. Mantle wedge overlying subduction zones is a good candidate (see Donnelly et al., 2004), but the metasomatic agent there may have an arc-melt signature (i.e., $[Nb/Th]_{PM\ (IAB)}<<1$ and $[Ta/U]_{PM\ (IAB)}<<1$), whereas oceanic basalts including incompatible element enriched OIB all have $[Nb/Th]_{PM\ (MORB,\ OIB)}>1$ and $[Ta/U]_{PM\ (MORB,\ OIB)}>1$ (Niu and Batiza, 1997; Niu et al., 1999). Following Niu et al. (2002) and Niu and O'Hara (2003), we suggest that the interface between the base of the growing oceanic lithosphere and the seismic low-velocity zone (LVZ) atop the asthenosphere is an ideal site for mantle metasomatism. Fig. 7 shows that oceanic lithosphere grows with time through basal accretion of the LVZ material (red arrows) before reaching its full thickness (after ~70 million years). The presence of a small amount of melt is required by and characterizes the LVZ (e.g., Lambert and Wyllie, 1968, 1970; Green, 1971; Green and Liebermann, 1976; Anderson, 1995; Niu and O'Hara, 2003; Niu, 2008). This melt would be enriched in volatiles (e.g., H_2O, CO_2) and incompatible elements (Niu et al., 2002; Niu and O'Hara, 2003). As the melt is buoyant at such depth range, it tends to concentrate as a melt-rich layer (in green; Fig. 7) towards the top of the LVZ. In the process of the lithosphere growth, the uppermost LVZ material forms spinel/garnet lherzolite as newly accreted lithosphere. Trapped low-F melts (from the melt-rich layer) collect and ascend, crystallizing liquidus minerals that add to the ambient peridotite (modal metasomatism), and leaving behind veins of garnet pyroxenite, hornblende–pyroxenite and hornblendite (yellow veins) before being finally absorbed in the ambient minerals (cryptic metasomatism) (O'Reilly and Griffin, 1988). A parcel of mantle (perhaps "plumes"?) ascends and partially melts by decompression when intersecting the solidus. These "plume" melts may gain incompatible element enrichments from the melt layer (in green; Fig. 7). Continued ascent of the "plume" melts through the lithosphere can assimilate earlier-formed metasomatic veins, leading to further enrichments of ultimately erupted OIB melts (Pilet et al., 2008; Niu, 2008). This may result in extremely enriched lavas such as alkali basalts, basanite and nephelinite on some ocean islands and intra-plate seamounts (Batiza and Vanko, 1984; Zindler et al., 1984). In this case, incompatible trace elements and radiogenic isotopes are often decoupled because the low-F melt metasomatism that has fractionated radioactive parent (P) and radiogenic daughter (D) element is recent, without having enough time to produce radiogenic isotopes (e.g., Sun and McDonough, 1989; Mahoney et al., 1994; Halliday et al., 1995; Niu et al., 1996, 1999; Niu and O'Hara, 2003).

It becomes conceptually apparent that "OIB sources" may in fact include constituents from the melt layer (green) and vein melts (Fig. 7)

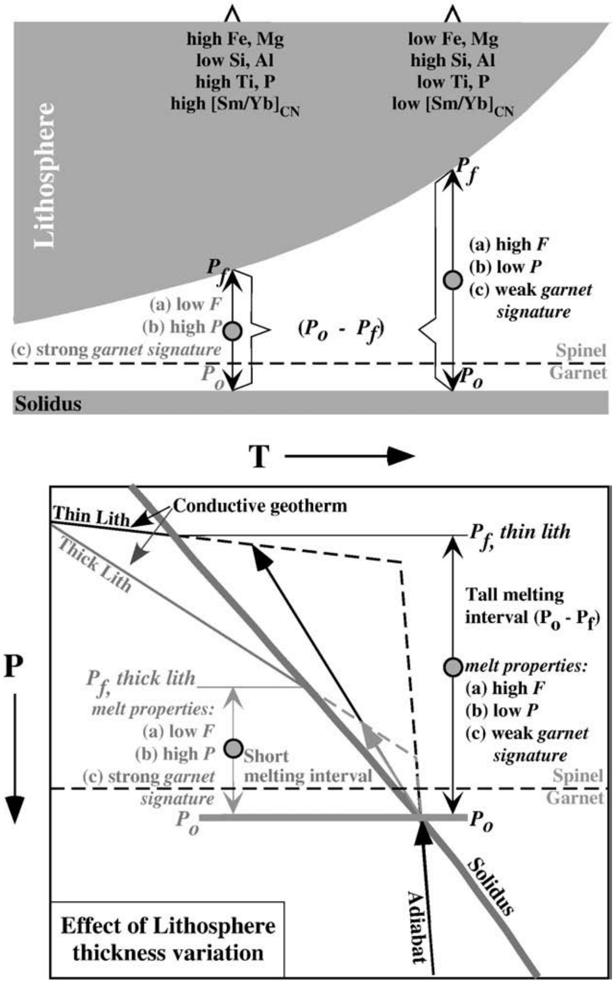

Fig. 6. Schematic illustration of the lid-effect concept to explain the OIB compositional variation as a function of the lithosphere thickness (Figs. 3 and 4). Top, the deep bound of the lithosphere constrains the final depth of melting (P_f) leading to subdued extent of melting by reducing the vertical range of decompression (P_o–P_f), which is proportional to the extent of melting. The mean pressure of melting recorded in the geochemistry of the erupted OIB melts is indicated by the filled circles, hence the inverse correlation between the extent and pressure of melting. Bottom, this concept is illustrated in pressure–temperature space. The adiabatically upwelling parcel of mantle begins to melt when intersecting the solidus at depth of P_o. Continued upwelling leads to continued decompression melting until the upwelling is ceased at P_f because of the lithosphere thickness constraint. The significance of all other elements is self-explanatory. Note that the solidus depth is assumed to be the same to illustrate the concept, but it is in fact unconstrained because of unconstrained fertile source composition and mantle potential temperature relevant to individual volcanic islands. Nevertheless, the lithosphere lid has the first-order OIB compositional control. Both panels are modified from Niu and Hékinian (1997), Niu et al. (2001) and Niu and O'Hara (2008).

as well as fertile mantle source materials from depth (plumes?). The fertile materials from depth may contain recycled "ancient" metasomatized oceanic lithosphere, which is an ideal candidate contributing to OIB petrogenesis (Niu and O'Hara, 2003). OIB lavas dominated by this component should show significant coupling between incompatible trace elements and radiogenic isotopes and even major elements (Hauri, 1996; Lassiter and Hauri, 1998; Castillo et al., 1998; Niu et al., 1999, 2002; Regelous et al., 1999; Wendt et al., 1999; Castillo et al., 2000).

6. Summary

(1) We have examined the global geochemical data set on ocean island basalts. We used the data on volcanic islands [a] whose eruption ages are available and [b] whose underlain lithosphere ages are either available or can be readily calculated, which allows calculation of the thickness of the oceanic lithosphere younger than ~70 million years at the time of volcanism. Furthermore, we only use samples with SiO_2<53 wt.%. This filtering resulted in a smaller data set with 115 volcanic islands from the Pacific, Atlantic and Indian Oceans, and a total of 12,996 samples for major element analyses. For trace elements, we only examined La/Sm and Sm/Yb ratios (normalized) to avoid the effect of crystal fractionation. We thus have 4710 samples for La/Sm ratio and 4607 samples for Sm/Yb ratio from these volcanic islands.

(2) We corrected the major element oxides of these samples further for fractionation effect to $Mg^{\#}=0.72$ (see Appendix A) using MORB LLDs and OIB LLDs with similar results. The corrected data largely represent Moho-crossing OIB melt compositions, thus allowing discussion of the data in terms of mantle (vs. crustal) processes. To reveal first-order OIB geochemical systematics on a global scale, we used island-averaged data instead of individual samples. That is, we have 115 (islands) data points to work with.

(3) Despite the large compositional variability for samples from single volcanic islands, the island-averaged data show statistically significant trends as a function of lithosphere thickness. The systematic Si_{72} and Al_{72} decrease and Fe_{72} and Mg_{72} increase with increasing lithosphere thickness are consistent with increasing mean pressure of asthenospheric melting (e.g., Niu and Batiza, 1991; Niu, 1997; Walter, 1998) from beneath thin lithosphere to beneath thick lithosphere. On the other hand, the systematic Ti_{72} and P_{72} increase with increasing lithosphere thickness is consistent with decreasing mean extent of melting (Niu, 1997; Walter, 1998) towards beneath the thickened lithosphere. The significant $[La/Sm]_{CN}$ and $[Sm/Yb]_{CN}$ increase with increasing lithosphere thickness is also consistent with decreasing extent and increasing pressure of melting.

(4) Both the "low-F melt signature" (i.e., high Ti_{72}, P_{72} and $[La/Sm]_{CN}$) and "garnet signature" (i.e., high $[Sm/Yb]_{CN}$) are the strongest in melts erupted on the thickened lithosphere and are diluted with increasing extent of melting. These signatures are diluted less in melts produced by overall low extents of melting beneath thick lithosphere and are diluted more in melts by overall high extents of melting beneath thin lithosphere as a result of continued decompression melting in the spinel peridotite facies.

(5) Although the data do not allow establishment of initial depth (solidus depth) of OIB mantle melting, which is likely to vary depending on fertile source compositions and mantle potential temperature beneath individual islands, the data demonstrate that the thickness of the oceanic lithosphere exerts the primary control on first-order OIB compositional variation, i.e., the lithosphere lid effect (Niu and O'Hara, 2007), that limits the height of the melting columns, thus the mean extent and pressure of melting on a global scale.

(6) Fertile mantle compositional heterogeneity is also required to explain large OIB compositional variation within individual islands, between islands and island groups. The mantle source heterogeneity is likely to have multiple origins. An incipient melt in the LVZ and its metasomatic vein lithologies in the lithosphere can contribute to and explain the highly enriched alkali lavas (alkali basalts, basanite and nephelinite). Recycled metasomatized deep portions of oceanic lithosphere are the best candidate as enriched fertile mantle sources accounting for the overall incompatible element enriched geochemistry of OIB.

(7) Mantle potential temperature variation can affect OIB composition by influencing initial depth and extent of melting, but it cannot be constrained with the existing data.

Acknowledgements

It is our great pleasure to contribute to the special volume in honour of Roger Hékinian for his pioneering effort and life-long

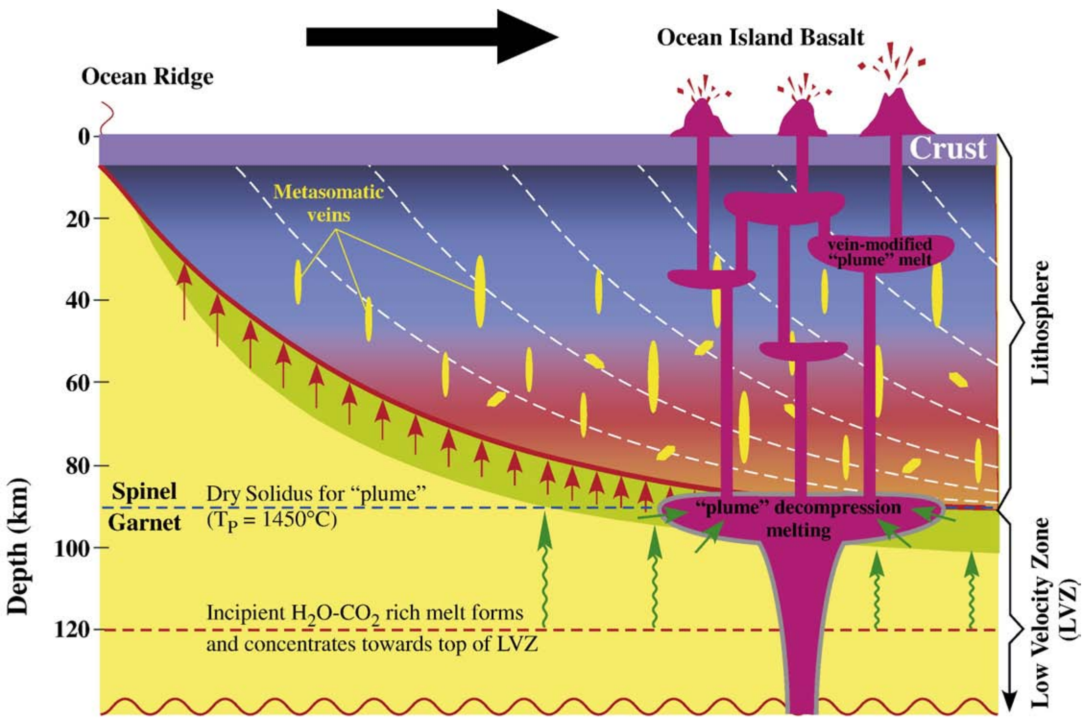

Fig. 7. Cartoon modified from Niu et al. (2002) and Niu (2008) to show that mantle metasomatism may take place at the interface between the growing lithosphere and the top of the LVZ where a melt-rich layer (green) may exist (Lambert and Wyllie, 1968, 1970; Green and Liebermann, 1976) and is enriched in volatiles (e.g., H_2O, CO_2) and incompatible elements (Niu and O'Hara, 2003, 2009-this issue). In the process of the lithosphere growth, this melt will also collect and ascend, crystallizing liquidus minerals added to the ambient peridotite (modal metasomatism), and leaving behind veins of pyroxenite and hornblendite (yellow veins) before being finally absorbed in the ambient minerals (cryptic metasomatism) (O'Reilly and Griffin, 1988). A parcel of mantle material (perhaps "plumes") ascends and partially melts by decompression when intersecting the solidus. These "plume" melts may gain incompatible element enrichments from the melt layer (green). Continued ascent of the "plume" melts through the lithosphere can assimilate the metasomatic veins formed earlier, leading to further enrichments of ultimately erupted OIB melts (Niu, 2008). (For interpretation of the references to colour in this figure legend, the reader is referred to the web version of this article.)

contributions to seafloor petrology and marine geology research. Y.N. thanks Roger for his support, friendship, encouragement and enjoyable research collaboration over the years. Discussion with Francis Albarède, Fred Frey, David Clague, Al Hofmann, Cin-Ty Lee, Yan Liang, Bill McDonough, Mike O'Hara, Vincent Salters, Alex Sobolev, Bill White, Peter Wyllie and Youxue Zhang has been useful. Y.N. also thanks the Leverhulme Trust for a Research Fellowship. Much of the work presented here is E.H.'s MSc research project completed at Durham University. E.H. wishes to thank Michael Williams for his help and support. We thank Nelson Eby (Editor), Karsten Haase and Sebastian Pilet for constructive comments that have helped improve the paper.

Appendix A. Supplementary data

Supplementary data associated with this article can be found, in the online version, at doi:10.1016/j.lithos.2009.04.038.

References

Albarède, F., 1998. Time-dependent models of U–Th–He and K–Ar evolution and the layering of mantle convection. Chemical Geology 145, 413–429.
Allègre, C.J., Hart, S.R., Minster, J.-F., 1983. Chemical structure and evolution of the mantle and continents determined by inversion of Nd and Sr isotopic data, I. Theoretical methods. Earth and Planetary Science Letters 66, 177–190.
Anderson, D.L., 1994. The sublithospheric mantle as the source of continental flood basalts. Earth and Planetary Science Letters 123, 269–280.
Anderson, D.L., 1995. Lithosphere, asthenosphere, and perisphere. Reviews of Geophysics 33 (125), 149.
Anderson, D.L., 2002. Plate tectonics as a far-from-equilibrium self-organized system. Geophysics Series 30, 411–425.
Anderson, D.L., Natland, J.H., 2005. A brief history of the plume hypothesis and its competitors: concept and controversy. In: Foulger, G.R., Natland, J.H., Presnall, D. C., Anderson, D.L. (Eds.), Plates, Plumes and Paradigms: Geological Society of America Special Paper, vol. 388, pp. 119–145.
Anderson, D.L., 2005. Scoring hotspots: the plume and plate paradigms. In: Foulger, G.R., Natland, J.H., Presnall, D.C., Anderson, D.L. (Eds.), Plates, Plumes and Paradigms: Geological Society of America Special Paper, vol. 388, pp. 31–54.
Armstrong, R.L., 1968. A model for the evolution of strontium and lead isotopes in a dynamic Earth. Review of Geophysics 6, 175–200.
Azevedo, J.M.M., Ferreira, M.R.P., 2006. The volcanotectonic evolution of Flores Island, Azores (Portugal). Journal of Volcanology and Geothermal Research 156, 90–102.
Batiza, R., 1980. The origin and petrology of young oceanic central volcanoes: are most tholeiitic rather than alkalic? Geology 8, 447–482.
Batiza, R., Vanko, D., 1984. Petrology of Pacific seamounts. Journal of Geophysical Research 89, 11235–11260.
Batiza, R., Melson, W.G., O'Hearn, T., 1988. Simple magma supply geometry inferred beneath a segment of the Mid-Atlantic Ridge 26°S. Nature 335, 428–431.
Batiza, R., Niu, Y.L., 1992. Petrology and magma chamber processes at the East Pacific Rise ~9°30′N. Journal of Geophysical Research 97, 6779–6797.
Blundy, J.D., Falloon, T.J., Wood, B.J., Dalton, J.A., 1995. Sodium partitioning between clinopyroxene and silicate melts. Journal of Geophysical Research 100, 15501–15515.
Bonneville, A., 2002. The Cook-Austral Volcanic Chain. www.mantleplumes.org.
Brodholt, J.P., Batiza, R., 1989. Global systematics of unaveraged zero-age MORB, comment on "Global correlations of ocean ridge basalt with axial depth and crustal thickness" by Klein, E.M., Langmuir, C.H. Journal of Geophysical Research 94, 4231–4239.
Burke, K., 2001. Origin of the Cameroon line of volcano-capped swells. Journal of Geology 109, 349–362.
Calmant, S., Cazenave, A., 1986. The effective elastic lithosphere under the Cook-Austral and Society islands. Earth and Planetary Science Letters 77, 187–202.
Calvert, A.T., Moore, R.B., McGeehin, J.P., Rodrigues da Silva, A.M., 2006. Volcanic history and Ar/Ar and C geochronology of Terceira island, Azores, Portugal. Journal of Volcanology and Geothermal Research 156, 103–115.
Campbell, I.H., 2005. Large igneous provinces and the mantle plume hypothesis. Element 1, 265–270.
Campbell, I.H., Griffiths, R.W., 1990. Implications of mantle plume structure for the evolution of flood basalts. Earth and Planetary Science Letters, 99, 79–83.
Caplan-Auerbach, J., Dunnebier, F., Ito, G., 2000. Origin of intraplate volcanoes from guyot heights and oceanic paleodepth. Journal of Geophysical Research 105, 2679–2697.
Carracedo, J.C., Day, S., Guillou, H., Rodriguez Badiolas, E.R., Canas, J.A., Perez Torrado, F.J., 1998. Hotspot volcanism close to a passive continental margin: the Canary Islands. Geological Magazine 135, 591–604.
Carracedo, J.C., Pérez, F.J., Ancochea, E., Meco, J., Hernán, F., Cubas, C.R., Casillas, R., Rodriguez, E., Ahijado, A., 2002. Cenozoic volcanism II: the Canary Islands. In:

Gibbons, W., Moreno, T. (Eds.), The Geology of Spain. Geological Society of London, pp. 439–472.
Castillo, P.R., Natland, J.H., Niu, Y.L., Lonsdale, P., 1998. Sr, Nd, and Pb isotopic variation along the Pacific ridges from 53 to 56°S: implications for mantle and crustal dynamic processes. Earth and Planetary Science Letters 154, 109–125, 1998.
Castillo, P.R., Klein, E., Bender, J., Langmuir, C., Shirey, S., Batiza, R., White, W., 2000. Petrology and Sr, Nd, and Pb isotope geochemistry of mid-ocean ridge basalt glasses from the 11°45′N to 15°00′N segments of the East Pacific Rise. Geochemistry Geophysics Geosystem 1 1999GC000024.
Castillo, P.R., Scarsi, P., Craig, H., 2007. He, Sr, Nd, and Pb isotopic constraints on the origin of the Marquesas and other linear volcanic chains. Chemical Geology 240, 205–221.
Chauvel, C., Hofmann, A.W., Vidal, P., 1992. HIMU EM—the French Polynesian connection. Earth and Planetary Science Letters 110, 99–119.
Clouard, V., Bonneville, A., 2004a. Ages of Seamounts, Islands and Plateaus on the Pacific Plate. version 2.1 www.mantleplumes.org.
Clouard, V., Bonneville, A., 2004b. In: Hekinian, R. (Ed.), Importance of submarine landslides in French Polynesia. Springer-Verlag, Oceanic Hotspots, pp. 209–238.
Coffin, M.F., Eldholm, O., 1994. Large igneous provinces: crustal structure, dimensions and external consequences. Review of Geophysics 32, 1–36.
Coffin, M.F., Pringle, M.S., Duncan, R.A., Gladczenko, T.P., Storey, M., Muller, R.D., Gahagan, L.A., 2002. Kerguelen hotspot magma output since 130 Ma. Journal of Petrology 43, 1121–1139.
Courtillot, V., Davaille, A., Besse, J., Stock, J., 2003. Three distinct types of hotspots in the Earth's mantle. Earth and Planetary Science Letters 205, 295–308.
Davies, G.F., 1999. Dynamic Earth: Plates, Plumes and Mantle Convection. Cambridge University Press, Cambridge. 460 pp.
Davies, G.F., 2005. A case for mantle plumes. Chinese Science Bulletin 50, 1541–1554.
DeMets, C., Gordon, R.G., Argus, D.F., Stein, S., 1990. Current plate motions. Geophysical Journal International 101, 425–478.
DeMets, C., Gordon, R.G., Argus, D.F., Stein, S., 1994. Effect of recent revisions to the geomagnetic reversal time scale on estimate of current plate motions. Geophysical Research Letters 21, 2191–2194.
Dick, H.J.B., Fisher, R.L., Bryan, W.B., 1984. Mineralogical variability of the uppermost mantle along mid-ocean ridges. Earth and Planetary Science Letters 69, 88–106.
Doell, R.R., Dalrymple, G.B., 1973. Potassium–argon ages and paleomagnetism of the Waianae and Koolau volcanic series, Oahu, Hawaii. Geological Society of America Bulletin 84, 1217–1242.
Donnelly, K.E., Goldstein, S.L., Langmuir, C.H., Spiegelman, M., 2004. Origin of enriched ocean ridge basalts and implications for mantle dynamics. Earth and Planetary Science Letters 226, 347–366.
Duncan, R.A., Richards, M.A., 1991. Hotspots, mantle plumes, flood basalts, and true polar wander. Review of Geophysics 1991, 29, 31–50.
Ellam, R.M., 1992. Lithosphere thickness as a control on basalt geochemistry. Geology 20, 153–156.
Esser, R.P., Kyle, P.R., McIntosh, W.C., 2004. $^{40}Ar/^{39}Ar$ dating of the eruptive history of Mount Erebus, Antarctica: volcano evolution. Bulletin of Volcanology 66, 671–686.
Farley, K.A., Natland, J.H., Craig, H., 1992. Binary mixing of enriched and undegassed (primitive?) mantle components (He, Sr, Nd, Pb) in Samoan basalts. Earth and Planetary Science Letters 111, 183–199.
Fekiacova, Z., Abouchami, W., Galer, S.J.G., Garcia, M.O., Hofmann, A.W., 2007. Origin and temporal evolution of Koolau Volcano, Hawaii: inferences from isotope data on the Koolau Scientific Drilling Project (KSDP), the Honolulu volcanics and ODP Site 843. Earth Planetary Science Letters 261, 65–83.
Feraud, G., Ishiro, K., Allegre, C.J., 1980. K/Ar ages and stress pattern in the Azores: geodynamic implications. Earth and Planetary Science Letters 46, 275–286.
Foulger, G.R., 2005. Mantle plumes: why the current skepticism? Chinese Science Bulletin 50, 1555–1560.
Foulger, G.R., Natland, J.H., Presnall, D.C., Anderson, D.L. (Eds.), 2005. Plates, Plumes, and Paradigms, vol. 388. Geological Society of America, Special Papers. 88app.
Franca, Z.T.M., Tassinari, C.C.G., Cruz, J., Aparicio, A.Y., Rodrigues, B.N., 2006. Petrology, geochemistry and Sr–Nd–Pb isotopes of the volcanic rocks from Pico island-Azores (Portugal). Journal of Volcanology and Geothermal Research 156, 71–89.
Frey, F.A., 1980. The origin of pyroxenites and garnet pyroxenites from Salt Lake Crater, Oahu, Hawaii, trace element evidence. American Journal of Science 280A, 427–499 1980.
Frey, F.A., Green, D.H., 1974. The mineralogy, geochemistry, and origin of lherzolite. Geochimica et Cosmochimica Acta 38, 1023–1059, 1974.
Frey, F.A., Green, D.H., 1978. Integrated models of basalt petrogenesis: a study of quartz tholeiites to olivine melilitites from south eastern Australia utilizing geochemical and experimental petrological data. Journal of Petrology 3, 463–513 1978.
Frey, F.A., Rhodes, J.M., 1993. Intershield geochemical differences among Hawaiian volcanoes: implications for source compositions, melting process and magma ascent paths. Philosophical Transaction of the Royal Society of London A342, 121–136.
Frey, F.A., Suen, C.J., Stockman, H., 1985. The Ronda high temperature peridotite: geochemistry and petrogenesis. Geochimica Cosmochimica Acta 49, 2469–2491.
Gast, P.W., 1968. Trace element fractionation and the origin of tholeiitic and alkaline magma types. Geochimimica et Cosmochimica Acta 32, 1055–1086.
Geldmacher, J., Hoernle, K., Bogaard, P.v.d., Duggen, S., Werner, R., 2005. New $^{40}Ar/^{39}Ar$ age and geochemical data from seamounts in the Canary and Maderia volcanic provinces: support for the mantle plume hypothesis. Earth and Planetary Science Letters 237, 85–101.
Green, D.H., 1971. Composition of basaltic magmas as indicators of conditions of origin: application to oceanic volcanism. Philosophical Transaction of the Royal Society of London A268, 707–725.
Green, D.H., 1973. Experimental melting studies on a model upper mantle composition at high pressure under water saturated and under-saturated conditions. Earth and Planetary Science Letters 19, 37–53.
Green, D.H., Liebermann, R.C., 1976. Phase equilibria and elastic properties of a Pyrolite model for the oceanic upper mantle. Tectonophysics 32, 61–92.
Green, D.H., Falloon, T.J., 2005. Primary magmas at mid-ocean ridges, 'hotspots,' and other intraplate settings: constraints on mantle potential temperature. In: Foulger, G.R., Natland, J.H., Presnall, D.C., Anderson, D.L. (Eds.), Plates, Plumes, and Paradigms: Geological Society of America Special Papers, vol. 388, pp. 217–248.
Green, D.H., Falloon, T.J., Eggins, S.M., Yaxley, G.M., 2001. Primary magmas and mantle temperatures. European Journal of Mineralogy 13, 437–451.
Griffiths, R.W., Campbell, I.H., 1990. Stirring and structure in mantle plumes. Earth and Planetary Science Letters 99, 66–78.
Gripp, A.E., Gordon, R.G., 2002. Young tracks of hotspots and current plate velocities. Geophysical Journal International 150, 321–361.
Haase, K.M., 1996. The relationship between the age of the lithosphere and the composition of oceanic magmas: constraints on partial melting, mantle sources and the thermal structure of the plates. Earth and Planetary Science Letters 144, 75–92.
Haase, K.M., Devey, C.W., Mertz, D.F., Stoffers, P., Garbe-Schonberg, D., 1996. Geochemistry of lavas from Mohns ridge, Norwegian–Greenland sea: implications for melting conditions and magma sources near Jan Mayen. Contributions to Mineralogy and Petrology 123, 223–237.
Haase, K.M., Mertz, D.F., Sharp, W.S., Garbe-Schönberg, C.-D., 2000. Sr–Nd–Pb isotope ratios, geochemical compositions, and $^{40}Ar/^{39}Ar$ data of lavas from San Felix Island (Southeast Pacific): implications for magma genesis and sources. Terra Nova 12, 90–96.
Halliday, A.N., Dickin, A.P., Fallick, A.E., Fitton, J.G., 1988. Mantle dynamics: a Nd, Sr, Pb and O isotopic study of the Cameroon line volcanic chain. Journal of Petrology 29, 181–211.
Halliday, A.N., Lee, D.-C., Tommasini, S., Davies, G.R., Paslick, C.R., Fitton, J.G., James, D.E., 1995. Incompatible trace elements in OIB and MORB source enrichment in the sub-oceanic mantle. Earth and Planetary Science Letters 133, 379–395.
Hamilton, W.B., 2002. The closed upper-mantle circulation of plate tectonics. Geophysics Series 30, 359–410.
Hanan, B.B., Graham, D.W., 1996. Lead and helium isotope evidence from oceanic basalts for a common deep source of mantle plumes. Science 272, 991–995.
Hart, S.R., Hauri, E.H., Oschmann, L.A., Whitehead, J.A., 1992. Mantle plumes and entrainment: isotopic evidence. Science 256, 517–520.
Hauri, E.H., 1996. Major element variability in the Hawaiian mantle plume. Nature 382, 415–419.
Helz, R.T., 1987. Differentiation behavior of Kilauea Iki lava lake, Kilauea Volcano, Hawaii: an overview of past and current work. The Geochemical Society Special Publication 1, 241–258.
Herzberg, C., O'Hara, M.J., 2002. Plume-associated ultramafic magmas of Phanerzoic age. Journal of Petrology 43, 1857–1883 2002.
Herzberg, C., Asimow, P.D., Arndt, N., Niu, Y.L., Lesher, C.M., Fitton, J.G., Cheadle, M.J., Saunders, A.D., 2007. Temperatures in ambient mantle and plumes: constraints from basalts, picrites and komatiites. Geochemistry, Geophysics, Geosystems 8. doi:10.1029/2006GC001390.
Hirschmann, M.M., Stolper, E.M., 1996. A possible role for garnet pyroxenite in the origin of the 'garnet signature' in MORB. Contributions to Mineralogy and Petrology 124, 185–208.
Hofmann, A.W., 1988. Chemical differentiation of the Earth: the relationship between mantle, continental crust, and oceanic crust. Earth and Planetary Science Letters 90, 297–314.
Hofmann, A.W., 1997. Mantle geochemistry: the message from oceanic volcanism. Nature 385, 219–229.
Hofmann, A.W., White, W.M., 1982. Mantle plumes from ancient oceanic crust. Earth and Planetary Science Letters 57, 421, 436.
Ingle, S., Weis, D., Doucet, S., Mattielli, N., 2003. Hf isotope constraints on mantle sources and shallow-level contaminants during Kerguelen hot spot activity since ~120 Ma. Geochemistry, Geophysics, Geosystems 4. doi:10.1029/2002GC000482.
Irving, A.J., Frey, F.A., 1978. Distribution of trace elements between garnet megacrysts and host volcanic liquids of kimberlitic to rhyolitic composition. Geochimica et Cosmochimica Acta 42, 771–787.
Jaques, A.L., Green, D.H., 1980. Anhydrous melting of peridotite at 0–15 kb pressure and the genesis of tholeiitic basalts. Contributions to Mineralogy and Petrology 73, 287–310.
Julian, B.R., 2005. What can seismology say about hotspots? In: Foulger, G.R., Natland, J.H., Presnall, D.C., Anderson, D.L. (Eds.), Plates, Plumes and Paradigms: Geological Society of America Special Paper, 388, pp. 155–170.
Kamenetsky, S., Everard, J.L., Crawford, A.J., Varne, R., Eggins, S.M., Lanyon, R., 2000. Enriched end-member of primitive MORB melts: petrology and geochemistry of glasses from Macquarie Island (SW Pacific). Journal of Petrology 41, 411–430.
Kerr, A., 2005. Oceanic LIPs: the kiss of depth. Element 1, 289–292.
Klein, E.M., Langmuir, C.H., 1987. Global correlations of ocean ridge basalt chemistry with axial depth and crustal thickness. Journal of Geophysical Research 92, 8089–8115.
Konter, J.G., Staudigel, H., Blichert-Toft, J., Hanan, B.B., Polvé, M., Davies, G.R., Shimizu, N., Schiffman, P., 2009. Geochemical stages at Jasper Seamount and the origin of intraplate volcanoes. Geochemistry, Geophysics and Geosystems 10, Q02001 doi. org/10.1029/2008GC002236.
Koppers, A.A.P., Russell, J.A., Jackson, M.G., Konter, J., Staudigel, H., Hart, S.R., 2008. Samoa reinstated as a primary hotspot trail. Geology 36, 435–438.
Lambert, I.B., Wyllie, P.J., 1968. Stability of hornblende and a model for the low velocity zone. Nature 219, 1240–1241.

Lambert, I.B., Wyllie, P.J., 1970. Low-velocity zone of the Earth's mantle—incipient melting caused by water. Science 169, 764–766.

Lassiter, J.C., Hauri, E.H., 1998. Osmium-isotope variations in Hawaiian lavas: evidence for recycled oceanic lithosphere in the Hawaiian plume. Earth and Planetary Science Letters 164, 483–496.

Lehnert, K., Su, Y., Langmuir, C.H., Sarbas, B., Nohl, U., 2000. A global geochemical database structure for rocks. Geochemistry, Geophysics and Geosystems 1. doi:10.1029/1999GC000026.

Le Maitre, R.W., 1989. A Classification of Igneous Rocks and Glossary of Terms. Blackwell Scientific Publications Ltd, Oxford, UK. 193pp.

Le Roex, A.P., Dick, H.J.B., Erlank, A.L., Reid, A.M., Frey, F.A., Hart, S.R., 1983. Geochemistry, mineralogy and petrogenesis of lavas erupted along the southwest Indian Ridge between the Bouvet Triple Junction and 11 degrees east. Journal of Petrology 24, 267–318.

Lloyd, F.E., Bailey, D.K., 1975. Light element metasomatism of the continental mantle: the evidence and the consequences. Physics and Chemistry of the Earth 9, 389–416.

Mahoney, J.J., Sinton, J.M., Kurz, D.M., Macdougall, J.D., Spencer, K.J., Lugmair, G.W., 1994. Isotope and trace element. Earth and Planetary Science Letters 121, 173–193.

Mcdonald, G.A., Katsura, T., 1964. Chemical composition of Hawaiian lavas. Journal of Petrology 5, 82–133.

McKenzie, D.P., Parker, R.L., 1967. The north Pacific: an example of tectonics on a sphere. Nature 216, 1276–1280.

McKenzie, D., Bickle, M.J., 1988. The volume and composition of melt generated by extension of the lithosphere. Journal of Petrology 29, 625–679.

McKenzie, D., O'Nions, R.K., 1995. The source regions of oceanic island basalts. Journal of Petrology 36, 133–159.

McKenzie, D.P., Jackson, J., Priestley, K., 2005. Thermal structure of oceanic and continental lithosphere. Earth and Planetary Science Letters 233, 337–349.

Meibom, A., Anderson, D.L., 2003. The statistical upper mantle assemblage. Earth and Planetary Science Letters 217, 123–139.

Menzies, M.A., Hawkesworth, C.J., 1987. Mantle metasomatism. Academic Press, London.

Montelli, R., Nolet, G., Dahlen, F.A., Masters, G., Engdahl, E.R., Hung, S.-H., 2004. Finite, frequency tomography reveals a variety of plumes in the mantle. Science 303, 338–343.

Morgan, W.J., 1968. Rises, trenches, great faults and crustal blocks. Journal of Geophysical Research 73, 1959–1982.

Morgan, W.J., 1971. Convection plumes in the lower mantle. Nature 230, 42–43.

Morgan, W.J., 1972. Plate motions and deep mantle convection. Geological Society of America Memoir 132, 7–22.

Muller, R.D., Roest, W.R., Royer, J.Y., Gahagan, L.M., Sclater, J.G., 1997. Digital isochrons of the world's ocean floor. Journal of Geophysical Research 102, 3211–3214.

Niu, Y.L., 1997. Mantle melting and melt extraction processes beneath ocean ridges: evidence from abyssal peridotites. Journal of Petrology 38, 1047–1074.

Niu, Y.L., 2004. Bulk, rock major and trace element compositions of abyssal peridotites: implications for mantle melting, melt extraction and post, melting processes beneath ocean ridges. Journal of Petrology 45, 2423–2458.

Niu, Y.L., 2005a. On the great mantle plume debate. Chinese Science Bulletin, 50, 1537–1540.

Niu, Y.L., 2005b. Generation and evolution of basaltic magmas: some basic concepts and a hypothesis for the origin of the Mesozoic, Cenozoic volcanism in eastern China. Geological Journal of China Universities 11, 9–46.

Niu, Y.L., 2008. The origin of alkaline lavas. Science 320, 883–884.

Niu, Y.L., Batiza, R., 1991. An empirical method for calculating melt compositions produced beneath mid, ocean ridges: application for axis and off, axis (seamounts) melting. Journal of Geophysical research 96, 21753–21777.

Niu, Y.L., Batiza, R., 1993. Chemical variation trends at fast and slow spreading ridges. Journal of Geophysical Research 98, 7887–7902.

Niu, Y.L., Batiza, R., 1994. Magmatic processes at a slow-spreading ridge segment—26°S Mid-Atlantic Ridge. Journal of Geophysical Research 99, 19719–19740.

Niu, Y.L., Batiza, R., 1997. Trace element evidence from seamounts for recycled oceanic crust in the eastern equatorial Pacific mantle. Earth and Planetary Science Letters 148, 471–484.

Niu, Y.L., Hékinian, R., 1997. Spreading rate dependence of the extent of mantle melting beneath ocean ridges. Nature 385, 326–329.

Niu, Y.L., Humphreys, E.R., 2008. Lithosphere thickness control on the extent and pressure of mantle melting beneath intraplate ocean islands. EOS Transactions AGU 89 (53), V43F–2196 Fall Meeting Supplement, Abstract.

Niu, Y.L., O'Hara, M.J., 2003. Origin of ocean island basalts: a new perspective from petrology, geochemistry and mineral physics considerations. Journal of Geophysical Research 108 (B4), 2209. doi:10.1029/2002JB002048.

Niu, Y.L., O'Hara, M.J., 2007. Varying Ni in OIB olivines—product of process not source. Geochimica et Cosmochimica Acta 71, a721-a721.

Niu, Y.L., O'Hara, M.J., 2008. Global correlations of ocean ridge basalt chemistry with axial depth: a new perspective. Journal of Petrology 49, 633–664.

Niu, Y.L., O'Hara, M.J., 2009. MORB Mantle Hosts the Missing Eu (Sr, Nb, Ta and Ti) in the Continental Crust: New Perspectives on Crustal Growth, Crust–mantle Differentiation and Chemical Structure of Oceanic Upper Mantle. Lithos 112, 1–17 (this issue).

Niu, Y.L., Waggoner, D.G., Sinton, J.M., Mahoney, J.J., 1996. Mantle source heterogeneity and melting processes beneath seafloor spreading centers: the East Pacific Rise, 18°–19°S. Journal of Geophysical Research 101, 27711–27733.

Niu, Y.L., Collerson, K.D., Batiza, R., Wendt, J.I., Regelous, M., 1999. Origin of enriched, type mid-ocean ridge basalt at ridges far from mantle plumes: the East Pacific Rise at 11°20′N. Journal of Geophysical Research 104, 7067–7087.

Niu, Y.L., Bideau, D., Hékinian, R., Batiza, R., 2001. Mantle compositional control on the extent of melting, crust production, gravity anomaly, ridge morphology, and ridge segmentation: a case study at the Mid, Atlantic Ridge 33°–35°N. Earth and Planetary Science Letters 186 (383), 399.

Niu, Y.L., Regelous, M., Wendt, J.I., Batiza, R., O'Hara, M.J., 2002. Geochemistry of near, EPR seamounts: importance of source vs. process and the origin of enriched mantle component. Earth and Planetary Science Letters 199, 327–345.

O'Nions, R.K., Evensen, N.M., Hamilton, P.J., 1979. Geochemical modeling of mantle differentiation and crustal growth. Journal of Geophysical Research 84, 6091–6101.

O'Reilly, Y.S., Griffin, W.L., 1988. Mantle metasomatism beneath western Victoria, Australia: I, Metasomatic processes in Cr-diopside lherzolites. Geochimica et Cosmochimica Acta 52, 433–447.

Parman, S.W., Kurz, M.D., Hart, S.R., Grove, T.L., 2005. Helium solubility in olivine and implications for high $^3He/^4He$ in ocean island basalts. Nature 437, 1140–1143.

Parsons, B., Sclater, J.G., 1977. An analysis of the variation of ocean floor bathymetry and heat flow with age. Journal of Geophysical Research 82, 803–827.

Pearce, J.A., Peate, D.W., 1995. Tectonic implications of the composition of volcanic arc magmas. Annual Review of Earth and Planetary Sciences 23, 251–285.

Phipps Morgan, J., Smith, W.F.S., 1992. Flattening of the sea-floor depth-age curve as a response to asthenospheric flow. Nature 359, 524–527.

Pilet, S., Hernandez, J., Sylvester, P., Poujol, M., 2005. The metasomatic alternative for ocean island basalt chemical heterogeneity. Earth and Planetary Science Letters 236, 148–166.

Pilet, S., Baker, M.B., Stolper, E.M., 2008. Metasomatized lithosphere and the origin of alkaline lavas. Science 320, 916–919.

Plank, T., Langmuir, C.H., 1998. The chemical compositions of subducting sediments and its consequences for the crust and mantle. Chemical Geology 145, 325–394.

Plesner, S., Holm, P.M., Wilson, J.R., 2002. ^{40}Ar–^{39}Ar geochronology of Sanro Antao, Cape Verde islands. Journal of Volcanology and Geothermal Research 120, 130-121.

Porcelli, D., Elliott, T., 2008. The evolution of He Isotopes in the convecting mantle and the preservation of high $^3He/^4He$ ratios. Earth and Planetary Science Letters 269, 175–185.

Prytulak, J., Elliott, T., 2007. TiO_2 enrichment in ocean island basalts. Earth Planetary Science Letters 263, 388–403.

Putirka, K.D., 2005. Mantle potential temperatures at Hawaii, Iceland, and the mid-ocean ridge system, as inferred from olivine phenocrysts: evidence for thermally driven mantle plumes. Geochemistry Geophysics Geosystem 6, Q05L08. doi:10.1029/2005GC000915.

Recq, M., Goslin, J., Charvis, P., Operto, S., 1998. Small-scale crustal variability within an intraplate structure: the Crozet Bank (southern Indian Ocean). Geophysical Journal International 134, 145–156.

Regelous, M., Niu, Y.L., Wendt, J.I., Batiza, R., Greig, A., Collerson, K.D., 1999. An 800 Ka record of the geochemistry of magmatism on the East Pacific Rise at 10°30′N: insights into magma chamber processes beneath a fast-spreading ocean ridge. Earth and Planetary Science Letters 168, 45–63.

Roeder, P.L., Emslie, R.F., 1970. Olivine^liquid equilibrium. Contributions to Mineralogy and Petrology 29, 275–289.

Rubin, K.H., Sinton, J.M., 2007. Inferences on mid-ocean ridge thermal and magmatic structure from MORB compositions. Earth and Planetary Science Letters 260, 257–276.

Rudnick, R.L., Gao, S., 2003. Composition of the continental crust. Treatise on Geochemistry 3, 1–64.

Salters, V.J.M., Hart, S.R., 1989. The hafnium paradox and the role of garnet in the source of mid-ocean ridge basalts. Nature 342, 420–422.

Schwartz, S., Klugel, A., Wohlgemuth-Ueberwasser, C., 2004. Melt extraction pathways and stagnation depths beneath the Maderia and Desertas rift zones (NE Atlantic) inferred from barometric studies. Contributions to Mineralogy and Petrology 140, 228–240.

Sen, G., Keshav, S., Bizimis, M., 2005. Hawaiian mantle xenoliths and magmas; composition and thermal character of the lithosphere. American Mineralogist 90, 871–887.

Smith, A.D., Lewis, C., 1999. The planet beyond the plume hypothesis. Earth Science Reviews 48, 135–182.

Stein, C.A., Stein, S., 1992. A model for the global variation in oceanic depth and heat-flow with lithospheric age. Nature 359, 123–129 1992.

Storevedt, K.M., Serralheiro, A., Moreira, M., Abranches, M.C., 1989. Magnetic structure and evolution of the island of Santa Maria, Azores. Physics of the Earth and Planetary Interiors 58, 228–238.

Sun, S.-s., Hanson, G.N., 1975. Origin of Ross Island basanitoids and limitations upon the heterogeneity of mantle sources for alkali basalts and nephelinites. Contributions to Mineralogy and Petrology 52, 77–106.

Sun, S.-s., McDonough, W.F., 1989. Chemical and isotopic systematics in ocean basalt: implication for mantle composition and processes. In: Saunders, A.D., Norry, M.J. (Eds.), Magmatism in the Ocean Basins, 42. Geological Society Special Publication, pp. 313–345.

Takazawa, E., Frey, F.A., Shimizu, N., Obata, M., 2000. Whole rock compositional variations in an upper mantle peridotite (Horoman, Hokkaido, Japan): are they consistent with a partial melting process? Geochimica et Cosmochimic Acta 64, 695–716.

Walter, M.J., 1998. Melting of garnet peridotite and the origin of komatiite and depleted lithosphere. Journal of Petrology 39, 29–60.

Wendt, J.I., Regelous, M., Niu, Y.L., Hekinian, R., Collerson, K.D., 1999. Geochemistry of lavas from the Garrett Transform Fault: insights into mantle heterogeneity beneath the eastern Pacific. Earth and Planetary Science Letters 173, 271–284.

White, R., McKenzie, D., 1989. Magmatism at rift zones: the generation of volcanic continental margins and flood basalts. Journal of Geophysical Research 94, 7685–7729.

White, W.M., Duncan, R.A., 1996. Geochemistry and geochronology of the Society Islands: new evidence for deep mantle recycling. American Geophysical Union Geophysical Monograph 95, 183–206.

Wilson, J.T., 1963a. A possible origin of the Hawaiian Islands. Canadian Journal of Physics 41, 863–870.
Wilson, J.T., 1963b. Evidence from islands on the spreading of the ocean floor. Nature 197, 536–538.
Wood, D.A., 1979. A variably veined suboceanic upper mantle—genetic significance for mid-ocean ridge basalts from geochemical evidence. Geology 7, 499–503.
Workman, R.K., Hart, S.R., Jackson, M., Regelous, M., Farley, K.A., Blusztajn, J., Kurz, M., Staudigel, H., 2004. Recycled metasomatised lithosphere as the origin of the enriched mantle II (EM2) end-member: evidence from the Samoan Volcanic Chain. Geochemistry, Geophysics and Geosystems 5 (4). doi:10.1029/2003GC00623.
Wright, T.L., Fiske, R.S., 1971. Origin of the differentiated and hybrid lavas of Kilauea volcano, Hawaii. Journal of Petrology, 12, 1–65.
Wyllie, P.J., 1971. Role of water in magma generation and initiation of diapiric uprise in the mantle. Journal of Geophysical Research 76, 1328–1338.
Zindler, A., Hart, S.R., 1986. Chemical geodynamics. Annual Review of Earth and Planetary Sciences 14, 493–571.
Zindler, A., Staudigel, H., Batiza, R., 1984. Isotope and trace element geochemistry of young Pacific seamounts: implications for the scale of mantle heterogeneity. Earth and Planetary Science Letters 70, 175–195.